TECHNICAL UNIVERSITY OF LIBEREC
FACULTY OF MECHATRONICS
AND INTERDISCIPLINARY ENGINEERING STUDIES

# PH. D. THESIS

LIBEREC 2006

PETR RÁLEK

Technical University of Liberec
Faculty of Mechatronics and Interdisciplinary Engineering Studies

Ph.D. Thesis

# Spectral Analysis of Discretized Model of Piezoelectric Resonator



Petr Rálek

Liberec, June 2006

Technická univerzita v Liberci
Fakulta mechatroniky a mezioborových inženýrských studií

Obor: Přírodovědné inženýrství

Dizertační práce

# Spektrální analýza diskretizovaného modelu piezoelektrického rezonátoru

Petr Rálek

Školitel: Prof. Ing. Jiří Maryška, CSc.

Rozsah práce:

Počet stran textu: 76
Počet tabulek: 2
Počet obrázků: 35

# Anotace

Předkládaná dizertační práce se zabývá modelováním rezonančních charakteristik piezoelektrických rezonátorů. Je uveden fyzikální popis piezolektrických materiálů s lineárními piezoelektrickými stavovými rovnicemi a definována úloha kmitání piezoelektrických rezonátorů. Následuje slabá formulace úlohy a její diskretizace metodou konečných prvků, která vede na zobecněnou úlohu vlastních čísel s řídkými a strukturovanými maticemi. Pro její řešení je použit implicitně restartovaný Arnoldiho algoritmus (IRA). Vyřešením algebraické úlohy lze nalézt rezonanční frekvence piezoelektrického rezonátoru. Pomocí koeficientů elektromechanické vazby jednotlivých módů jsou posléze vybrány dominantní módy kmitání.

Implementace modelu zahrnuje vytvoření geometrie rezonátoru, sestavení úlohy vlastních čísel, její řešení a následně identifikaci jednotlivých módů a jejich roztřídění dle významnosti. K tvorbě geometrie a sítě je použit volně dostupný software GMSH, pro řešení algebraické úlohy je použita implementace metody IRA z volně dostupné knihovny ARPACK. Ostatní součásti programové implementace jsou prací autora.

Program byl testován na podélném a torzním kmitání piezoelektrické tyčinky (s velmi dobrou shodou s analytickým řešením) a posléze na reálné úloze tloušťkově střižných kmitů planparalelního křemenného rezonátoru. Zde byly nalezeny správné dominantní módy kmitů, přičemž odchylka od naměřených rezonančních frekvencí činí asi 15%. Relativní odstup jednotlvých rezonančních frekvencí zůstal dobře zachován.

Motivací práce bylo navržení a implementace kompaktního softwarového modulu, který by mohl sloužit při procesu návrhu a výroby piezoelektrických prvků s požadovanými rezonančními vlastnostmi. Uvedenou odchylku od naměřených rezonančnch frekvencí lze odstranit kalibrací modelu na danou úlohu a, při uvážení kvalitativní správnosti výsledků modelu, lze tento v dané oblasti prakticky využívat.

# List of symbols

## Physical symbols and quantities

| Symbol, quantity | Unit | Descripiton |
|---|---|---|
| $c_{ijkl}$ | $N.m^{-2}$ | tensor of elastic modules |
| $\mathbb{C}$ | $N.m^{-2}$ | tensor of elastic modules in shortened indexation |
| $d_{ijk}$ | $C.m^{-2}$ | tensor of piezoelectric coefficients |
| $\mathbb{D}$ | $C.m^{-2}$ | tensor of piezoelectric coefficients in shortened indexation |
| $\varepsilon_{ij}$ | $N.V^{-1}.m^{-1}$ | permittivity tensor |
| $\mathcal{E}$ | $N.V^{-1}.m^{-1}$ | permittivity tensor in shortened indexation |
| $\varrho$ | $kg.m^{-3}$ | material density |
| $\mu$ | | Poisson's ratio |
| $G$ | $N.m^{-2}$ | effective torsional modulus |
| $\mathbf{u} = (u_1, u_2, u_3)$ | $m$ | displacement ($\tilde{\mathbf{u}}$ for time dependent displacement) |
| $\varphi$ | $V$ | electric potential ($\tilde{\varphi}$ for time dependent potential) |
| $Q$ | $C$ | electric charge |
| $\mathbf{S}$ | | strain tensor |
| $\mathbf{T}$ | $N.m^{-2}$ | stress tensor |
| $\mathbf{E}$ | $V.m^{-1}$ | electric field |
| $\mathbf{D}$ | $C.m^{-2}$ | electric displacement |
| $\omega$ | $Hz$ | circular frequency of oscillation |
| $f$ | $Hz$ | frequency of oscillation |
| $k$ | | coefficient of electromechanical coupling |
| $E_m$ | $J$ | mutual energy |
| $E_d$ | $J$ | dielectric energy |
| $E_{st}$ | $J$ | elastic energy |

## Mathematical symbols

| Symbol | Description |
|---|---|
| $\mathcal{R}$ | set of real numbers |
| $\mathcal{C}$ | set of complex numbers |
| i | complex unit |
| $\mathbf{x} = (x_1, x_2, ..., x_n)^T$ | column vector (space variable for $n = 3$) |
| $\delta_{ij}$ | Kronecker delta |
| U | column vector of nodal values in FEM |
| $\mathbb{A}$, $\mathbb{A}^T$ | matrix, transpose of matrix |
| $\mathbb{A}^{-1}$ | inverse of matrix $\mathbb{A}$ |
| $\mathbb{I}$ | identity matrix |
| $\lambda$ | eigenvalue |
| $\mathcal{K}_k(\mathbb{A}, \mathbf{x})$ | Krylov subspace generated by matrix $\mathbb{A}$ and vector $\mathbf{x}$ |
| $Span(\mathbf{x}_1, ..., \mathbf{x}_n)$ | linear hull of vectors $\mathbf{x}_1, ..., \mathbf{x}_n$ |
| $\Omega$ | domain in $\mathcal{R}^3$ |
| $\Gamma$ | boundary of domain $\Omega$, $\Gamma = \partial\Omega$ |
| $W_2^{(1)}$ | Sobolev function space |
| $L_2$ | Lebesgue space of square integrable functions |
| $C^{(k)}$ | space of functions continuous up to $k$-th derivation |
| $(.,.)_\Omega$ | scalar product on $\Omega$ |
| $< .,. >_\Gamma$ | scalar product on boundary $\Gamma$ |
| $\|.,.\|_\star$ | norm induced by scalar product $(.,.)_\star$ |
| $h$ | discretization parameter |
| $\mathcal{O}(h)$ | error function proportional to $h$ |
| $g$ | scalar function |
| $\mathbf{g} = (g_1, g_2, g_3)$ | vector function |
| $\frac{\partial g}{\partial x_i}$ | spatial derivative of $g$ with respect to $x_i$ |
| $\nabla = (\frac{\partial}{\partial x_1}, \frac{\partial}{\partial x_2}, \frac{\partial}{\partial x_3})$ | gradient operator |
| $\dot{g} = \frac{df}{dt}$ | time derivative of $g$ |
| $\ddot{g} = \frac{d^2 f}{dt^2}$ | second time derivative of $g$ |

## Abbreviations

| Abbreviation | Descripiton |
|---|---|
| BC | boundary conditions |
| FEM | finite element method |
| KSM | Krylov subspace methods |
| IRA | implicitly restarted Arnoldi algorithm |
| 1D, 2D, 3D | one–, two–, three–dimensional |

# Contents

# Introduction

## Piezoelectric materials and their usage

An interest in piezoelectric materials dates back to the end of the 19th century, when brothers Curie discovered the *direct piezoelectric effect* - compression of a piezoelectric crystal resulted in appearance of an electric charge on its surface. They later also described the *converse piezoelectric effect* - deformation caused by the electric field. During time, many materials, embodying the piezoelectric effect, were discovered, such as crystalline quartz, PZT ceramics, polymer composites (see, e.g., [36]).

In the 20's of the last century, the piezoelectric materials started its successful use in industry. They are used in measurement, inspecting systems, wave generation, etc... Among these applications, *piezoelectric resonators* play fundamental role.

**Piezoelectric resonators** Piezoelectric resonator is the thin stick or wafer made of the piezoelectric material, with two or more electrodes on its surface (see, e.g., [27]). In consequence of harmonic electric loading, the resonator oscillates. The most important parameters, describing the behavior of the resonator, are its *resonant frequencies* - frequencies of the oscillations with maximal amplitudes in some characteristic directions.

Not each of the oscillation modes can be excited with ease, many of them are partially absorbed due to the material and shape properties of a particular resonator. It is important to find such oscillation modes, which can be excited much more easily then the other ones. The resonator's working area then stands in the frequency interval about the dominant frequency.

Piezoelectric resonators are used, e.g., as stabilizers of frequencies of electric circuits, frequency filters, sensors of nonelectric quantities.

## Motivation of the thesis

In this paragraph we present motivation for our work. For piezoelectric materials, resonant frequencies are typically determined by experimental or analytical methods. Analytical methods are, however, applicable only for some particular, simply posed problems and simply shaped resonators. The main disadvantage of the experimental

testing is its high cost.

**The role of mathematical modelling** Mathematical models, depending on their complexity, can bridge over the above mentioned disadvantages of other methods. In last ten or fifteen years, the mathematical modelling of piezoelectric materials and the use of the finite element method (FEM) became obvious (although formulation of the method for piezoelectric materials by Allik and Hughes [1] dates back to 1970).

We mention several publications, which have opened different areas in the FEM computation of piezoelectric problems. In 1990, Lerch published the general formulation for two- and three- dimensional FEM and presented the numerical results for oscillations of piezoeceramic bar. Tzou, Tseng [24] (in 1991), Hwang, Park [8] (in 1993) or Samanta, Ray [17] (in 1996) presented the numerical results for active control of vibration of piezoelectric materials, using various higher order finite elements (for more detailed historical overview, see e.g. [15]). Moetakef [13] (in 1995) derived the higher order tetrahedral element, other higher order elements are described e.g. in [6]. Nowadays, also the shell elements based on the Mindlin's higher order plate theory are used (see e.g [25]).

**The goal of the thesis** In this work, we describe the finite element (FEM) model of the piezoelectric resonator based on the physical description of the piezoelectric material. Discretization of the problem then leads to a large sparse linear algebraic system, which defines the generalized eigenvalue problem. Resonant frequencies are subsequently found by solving this algebraic problem.

A core of this thesis is related to the particular generalized eigenvalue problem arising from discretization. Depending on the discretization parameters, this problem may become large, which may complicate application of standard techniques known from the literature. It should be pointed out, that typically we are not interested in all eigenvalues (resonant frequencies). For determining of several of them it seems therefore appropriate to consider iterative methods.

Based on the finite element discretization of the mathematical model, we wish to propose, implement and test numerical algorithms for computing several resonant frequencies of piezoelectric resonators, and compare our results with experimental measurements.

The main accent was put on the creation of the compact software module, which would be suitable for solving problems with resonators with various shapes and finding the dominant resonant frequencies.

The most expensive part (in time and also in money costs) in the design process of new resonators is the production of the prototypes and measurement of their basic resonant behavior. Therefore, the mathematical model can save both time and money and the results should be suitable in the design process of the resonators with requested resonant properties.

## Structure of the thesis

In the first chapter, the physical description of the piezoelectric materials is described, using the governing motion equations accomplished with the linear piezoelectric state equations. Along them, other necessary physical quantities and piezoelectric material properties are introduced.

The second chapter describes the mathematical formulation of the problem. The weak formulation and the use of the finite element method are presented.

Several different types of possible tasks in the area of modelling of the piezoelectric materials are given in the third chapter. The accent is put on the problem of free oscillation, governed by the generalized eigenvalue problem, and on the method for finding the dominant oscillation modes.

The fourth chapter presents the description of Krylov subspace methods (methods of numerical linear algebra), which would be suitable for solving the large eigenvalue problems, especially of the used implicitly restarted Arnoldi method.

The computer implementation of the model is a subject of the fifth chapter. It contains the brief survey of the programming work and the description of pre- and postprocessing phase of the computation.

The sixth chapter gives the results of experimental testing of the model. In two model examples of piezoelectric beam oscillation, the computed results showed a good agreement with the analytically solution.

The application of the model to the real problem of thickness-shear oscillation of the plan-parallel quartz resonator is included in the seventh chapter. The correspondence with measured results was pretty good in the qualitative way (specification of dominant oscillation modes). The total values of the dominant frequencies differed from the measurement approximately about 15 percents, but the relative distances of the particular oscillation modes were retained.

# Chapter 1

# Physical formulation of the problem

## 1.1 Physical description of piezoelectric materials

In this chapter, we mention some basic physical properties of the piezoelectric materials and then formulate the problem of oscillation of the piezoelectric resonator. Throughout the thesis, all vectors are considered column vectors.

### 1.1.1 Piezoelectric equations of state

A crystal made of piezoelectric material represents a structure, in which the deformation and electric field depend on each other. A deformation (impaction) of the crystal induces electric charge on the crystal's surface. On the other hand, subjecting the crystal to electric field causes its deformation. In linear theory of piezoelectricity, derived by Tiersten in [22], this process is described by two constitutive equations - the **generalized Hook's law** (1.1) and the **equation of the direct piezoelectric effect** (1.2),

$$\mathrm{T_{ij}} = c_{ijkl}\,\mathrm{S_{kl}} - d_{kij}\,\mathrm{E_k}, \qquad i,j = 1,2,3, \tag{1.1}$$

$$\mathrm{D}_k = d_{kij}\,\mathrm{S_{ij}} + \varepsilon_{kj}\,\mathrm{E_j}, \qquad k = 1,2,3. \tag{1.2}$$

Here, as in other similar terms throughout the thesis, we use the convention known as the Einstein's additive rule ($a_{ij}b_j = \sum_{j=1}^{3} a_{ij}b_j$, see e.g. [21]). The Hook's law (1.1) describes dependence between the **stress tensor T**, the **strain tensor S** and the **vector of intensity of electric field E**,

$$\begin{aligned} \mathrm{S}_{ij} &= \frac{1}{2}\left[\frac{\partial \tilde{u}_i}{\partial x_j} + \frac{\partial \tilde{u}_j}{\partial x_i}\right], \quad i,j = 1,2,3, \\ \mathrm{E_k} &= -\frac{\partial \tilde{\varphi}}{\partial x_k}, \qquad\qquad k = 1,2,3, \end{aligned}$$

where $\tilde{\mathbf{u}} = (\tilde{u}_1, \tilde{u}_2, \tilde{u}_3)^T$ is the **displacement vector** and $\tilde{\varphi}$ is the **electric potential**. The strain tensor $\mathbf{S}$ and the stress tensor $\mathbf{T}$ are symmetric [27]. The equation of the direct piezoelectric effect (1.2) describes the dependence between the **vector of electric displacement D**, the strain and the intensity of electric field. Quantities $c_{ijkl}$, $d_{kij}$ and $\varepsilon_{ij}$ represent symmetric material tensors, described in the next paragraph.

### 1.1.2 Material properties

Properties of the piezoelectric resonator, closely related to the resonator material, are characterized by the **material tensors**. The state equations (1.1) and (1.2) represent a linear approximation of the thermodynamic state equations, with tensors $c_{ijkl}$, $d_{kij}$ and $\varepsilon_{ij}$ playing role of the material constants. From the conditions of the thermodynamic stability ([18], part II), tensors $c_{ijkl}$ and $\varepsilon_{ij}$ have to be symmetric and positive definite.

The first of them is the **tensor of elastic modules**:

$$(c_{ijkl}), \quad i,j,k,l = 1,2,3.$$

It is a four order tensor, but due to its symmetry

$$c_{ijkl} = c_{jikl} = c_{ijlk} = c_{klij}, \tag{1.3}$$

it has generally only 21 independent components. In some cases, it is worth to use the shortened indexation of its components, which allows to simplify some formulations, and transform product of two tensors to the multiplication of a matrix and a vector (see e.g. [26]). Indeed, if we define the indices $\mu$, $\nu$ as

$$\begin{aligned} \mu &= i \quad \text{if} \quad i = j, \\ \mu &= 9 - i - j \quad \text{if} \quad i \neq j, \\ \nu &= k \quad \text{if} \quad k = l, \\ \nu &= 9 - k - l \quad \text{if} \quad k \neq l, \end{aligned} \tag{1.4}$$

then we can uniquely map the fourth order tensor $c_{ijkl}$ satisfying (1.3) into the matrix $c_{\mu\nu}$, and the matrix $\mathrm{T}_{ij}$ into the vector $\mathrm{T}_\mu$,

$$c_{\mu\nu} \equiv c_{ijkl}, \quad \mathrm{T}_\mu \equiv \mathrm{T}_{ij}, \quad \mu,\nu = 1,\ldots,6,$$

which, with the analogous notation

$$\begin{aligned} \mathrm{S}_\mu &\equiv \mathrm{S}_{ij} \quad \text{if} \quad i = j, \\ \mathrm{S}_\mu &\equiv 2\,\mathrm{S}_{ij} \quad \text{if} \quad i \neq j, \end{aligned}$$

gives

$$c_{ijkl}\,\mathrm{S}_{ij} = c_{\mu\nu}\,\mathrm{S}_\nu = (\mathbb{C}\mathrm{S})_\mu,$$

where

$$\mathbb{C} = (c_{\mu\nu})_{\mu,\nu=1}^{6} = \begin{bmatrix} c_{1111} & c_{1122} & c_{1133} & c_{1123} & c_{1131} & c_{1112} \\ c_{1122} & c_{2222} & c_{2233} & c_{2223} & c_{2231} & c_{2212} \\ c_{1133} & c_{2233} & c_{3333} & c_{3323} & c_{3331} & c_{3312} \\ c_{1123} & c_{2223} & c_{3323} & c_{2323} & c_{2331} & c_{2312} \\ c_{1131} & c_{2231} & c_{3331} & c_{2331} & c_{3131} & c_{1112} \\ c_{1112} & c_{2212} & c_{3312} & c_{2312} & c_{1112} & c_{1212} \end{bmatrix}, \tag{1.5}$$

$$\mathrm{S} = [\mathrm{S}_1, \mathrm{S}_2, \mathrm{S}_3, \mathrm{S}_4, \mathrm{S}_5, \mathrm{S}_6]^T.$$

$(\mathbb{C}\mathrm{S})_\mu$ denotes $\mu$-th component of resulting vector $\mathbb{C}\mathrm{S}$. The matrix $\mathbb{C}$ is symmetric and positive definite.

The three order **tensor of piezoelectric coefficients**

$$(d_{ijk}), \quad i,j,k = 1,2,3,$$

is symmetric in its last two indices,

$$d_{ijk} = d_{ikj},$$

and thus has only 18 independent components. The shortened indexation (1.4) gives

$$\begin{aligned} d_{i\mu} &\equiv d_{ijk}, \quad \text{for} \quad j = k = \mu = 1,2,3, \\ d_{i\mu} &\equiv 2d_{ijk} \quad \text{for} \quad j \neq k, \quad \mu = 4,5,6, \end{aligned}$$

and the second term on the right side of (1.1) can be written in the form

$$d_{ijk}\ \mathrm{E}_i = d_{i\mu}\ \mathrm{E}_i = (\mathbb{D}^T\mathrm{E})_\mu,$$

where

$$\mathbb{D} = (d_{i\mu})_{\mu=1..6,i=1,2,3} = \begin{bmatrix} d_{111} & d_{122} & d_{133} & 2d_{123} & 2d_{131} & 2d_{112} \\ d_{211} & d_{222} & d_{233} & 2d_{223} & 2d_{231} & 2d_{212} \\ d_{311} & d_{322} & d_{333} & 2d_{323} & 2d_{331} & 2d_{312} \end{bmatrix}. \tag{1.6}$$

Electric properties are described by the symmetric **permittivity tensor**

$$(\varepsilon_{ij}), \quad i,j = 1,2,3, \quad \varepsilon_{ij} = \varepsilon_{ji}.$$

It can be written as a matrix

$$\mathcal{E} = \begin{bmatrix} \varepsilon_{11} & \varepsilon_{12} & \varepsilon_{13} \\ \varepsilon_{12} & \varepsilon_{22} & \varepsilon_{23} \\ \varepsilon_{13} & \varepsilon_{23} & \varepsilon_{33} \end{bmatrix}. \tag{1.7}$$

Similarly to matrix $\mathbb{C}$, under the condition of thermodynamic stability, the matrix $\mathcal{E}$ is positive definite.

## 1.2 Oscillation and resonance of elastic materials

Before we describe an oscillation of the piezoelectric system, we briefly recall the general principles of oscillation in the case of pure elastic material (described e.g. in [4]). When an oscillatory system is skewed from the equilibrium and then it is let to oscillate without any further impact of outer forces, we observe a *free oscillation*. This oscillation can be decomposed to the set of *natural oscillations* with some particular frequencies, called *eigenfrequencies*. Free oscillation is a linear combination of natural oscillations.

Consider a system with *lumped parameters* with $n$ degrees of freedom. Free undamped oscillation of this system can be described by the motion equation [4, p. 121]

$$\mathbb{M}\,\ddot{\mathbf{u}} + \mathbb{K}\,\mathbf{u} = 0, \tag{1.8}$$

where $\mathbf{u}^T = [u_1, ..., u_n]$ is the time dependent displacement vector, $\mathbb{M}$ is the mass matrix and $\mathbb{K}$ is the stiffness matrix (both matrices are symmetric and positive definite). Assume the solution of (1.8) in the form

$$\mathbf{u}(t) = \mathbf{v}e^{i\omega t},$$

where $\mathbf{v}$ is the vector of amplitudes and $\omega$ is the angular frequency. Substituting $\mathbf{u}(t)$ in (1.8) gives

$$(\mathbb{K} - \lambda\mathbb{M})\,\mathbf{v} = 0, \quad \lambda \equiv \omega^2. \tag{1.9}$$

The matrix pencil $(\mathbb{K} - \lambda\mathbb{M})$ has $n$ real eigenvalues and set of $n$ linearly independent eigenvectors. To see this, let $\mathbb{M} = \mathbb{L}\mathbb{L}^T$ be the Choleski decomposition of matrix $\mathbb{M}$. Then (1.9) can be written as

$$\mathbb{K}\,\mathbf{v} = \lambda\mathbb{L}\mathbb{L}^T\,\mathbf{v},$$

which is equivalent to

$$\mathbb{L}^{-1}\mathbb{K}(\mathbb{L}^T)^{-1}\mathbb{L}^T\,\mathbf{v} = \lambda\mathbb{L}^T\,\mathbf{v}.$$

Matrix $\mathbb{L}^{-1}\mathbb{K}(\mathbb{L}^T)^{-1}$ is symmetric and thus has real eigenvalues and set of $n$ linearly independent eigenvectors $\mathbf{y}_1, ..., \mathbf{y}_n$. So has the matrix $\mathbb{M}^{-1}\mathbb{K}$, with eigenvectors $\mathbf{v}_i = (\mathbb{L}^T)^{-1}\,\mathbf{y}_i$. The eigenvectors $\mathbf{y}_1, ..., \mathbf{y}_n$ can be chosen to be orthonormal,

$$[\mathbf{y}_1, ..., \mathbf{y}_n]^T[\mathbf{y}_1, ..., \mathbf{y}_n] = \mathbb{I},$$

thus eigenvectors $\mathbf{v}_1, ..., \mathbf{v}_n$ are $\mathbb{M}$-orthonormal,

$$[\mathbf{v}_1, ..., \mathbf{v}_n]^T\,\mathbb{M}\,[\mathbf{v}_1, ..., \mathbf{v}_n] = \mathbb{I},$$

where $\mathbb{I}$ is identity matrix. The eigenvalues $\lambda_i$, $i \in \hat{n}$ of the matrix $\mathbb{M}^{-1}\mathbb{K}$ are squares of the eigenfrequencies $\omega_i$. The eigenvector $\mathbf{v}_i$ of the matrix $\mathbb{M}^{-1}\mathbb{K}$ and the eigenvalue $\lambda_i$ describe the $i$-th *mode* of natural oscillation (the eigenvector gives the amplitudes, which determine the shape of oscillation).

The system can also oscillate in consequence of periodical (usually harmonic) generation of vibration by inner or outer loading, which is called *forced oscillation.* We describe the principle of resonance in the case of forced undamped oscillation. System with $n$ degrees of freedom from the last example is governed by the motion equation [4, p. 127],

$$\mathbb{M}\,\ddot{\mathbf{u}} + \mathbb{K}\,\mathbf{u} = \mathbf{f}(t), \tag{1.10}$$

where $\mathbf{f}(t)$ is the vector of harmonic loading. Let

$$\mathbf{f}(t) = \mathbf{f}_0 \cos \omega t.$$

For steady harmonic loading, system oscillates with the frequency of loading and oscillation is called steady oscillation. Equation (1.10) represents the system of differential equations with a right hand side. Let the eigenvectors $\mathbf{v}_1, ..., \mathbf{v}_n$ of the matrix $\mathbb{M}^{-1}\mathbb{K}$ be $\mathbb{M}$-orthonormal. Then vector of amplitudes of steady undamped forced oscillation is given by [4, p. 128]

$$\mathbf{u}_0 = \sum_{i=1}^{n} \frac{\mathbf{v}_i \mathbf{v}_i^T}{\omega_i^2 - \omega^2}\, \mathbf{f}_0. \tag{1.11}$$

When the frequency $\omega$ approaches some eigenfrequency $\omega_i$ of the system, the $i-$th component in (1.11) goes to infinity. This case is called the *resonance.* Thus, the eigenfrequencies of the system are also called the *resonance frequencies* (further in the text, resonance frequency and eigenfrequency will mean the same). The solution of (1.10) has the form [4, p. 128],

$$\mathbf{u}(t) = \sum_{i=1}^{n} \frac{\mathbf{v}_i \mathbf{v}_i^T}{\omega_i^2 - \omega^2}\, \mathbf{f}_0 (\cos \omega t - \cos \omega_i t)$$

and for the resonance, $\omega \to \omega_i$, the $i$-th component of the sum is equal to

$$t\, \frac{\sin \omega_i t}{2\omega_i}\, \mathbf{v}_i \mathbf{v}_i^T \mathbf{f}_0,$$

and increases in time.

Computing of oscillation of the pure *elastic continuum* is solved by analytical methods or by discretization of the continuum into lumped parameters, for which motion equations are solved. The finite element method (FEM) represents nowadays one of the most important discretization method. It divides the continuum into finite elements, where values of unknown functions in nodes of division are approximated with the help of special basis functions. As a result a system similar to (1.8) is obtained. For description of widely used methods see e.g. in [4] or [14]. For piezoelectric continuum, oscillations of simply posed problems are usually solved by analytical methods (a survey of analytical methods is given in [27]). Experimental measurements are in many cases too expensive and therefore impractical. Mathematical modelling of more complicated settings require using of advanced numerical techniques. That is the motivation for using FEM. Its basic formulation was published by Allik back in 1970 [1], but the rapid progress in FEM modelling in piezoeletricity came in the last ten years (see the brief survey in paragraph ).

## 1.3 Oscillation of piezoelectric continuum

Consider resonator made of piezoelectric material with density $\varrho$, characterized by material tensors. We denote the volume of the resonator as $\Omega$ and its boundary as $\Gamma$. Behavior of the piezoelectric continuum is governed, in some time range $[0, \mathrm{T}]$, by two differential equations: Newton's law of motion (1.12) and the quasi-static approximation of Maxwell's equation (1.13) (see, e.g., [12]),

$$\varrho \frac{\partial^2 \tilde{u}_i}{\partial t^2} = \frac{\partial \mathrm{T_{ij}}}{\partial x_j} \qquad i = 1,2,3, \qquad x \in \Omega, \quad \mathrm{t} \in (0, \mathrm{T}), \tag{1.12}$$

$$\nabla . \, \mathbf{D} = \frac{\partial \mathrm{D_j}}{\partial x_j} = 0. \tag{1.13}$$

Replacement of $\mathbf{T}$, resp. $\mathbf{D}$ in (1.12) and (1.13) with the expressions (1.1), resp. (1.2), gives

$$\varrho \frac{\partial^2 \tilde{u}_i}{\partial t^2} = \frac{\partial}{\partial x_j} \left( c_{ijkl} \, \frac{1}{2} \left[ \frac{\partial \tilde{u}_k}{\partial x_l} + \frac{\partial \tilde{u}_l}{\partial x_k} \right] + d_{kij} \, \frac{\partial \tilde{\varphi}}{\partial x_k} \right) \qquad i = 1,2,3, \tag{1.14}$$

$$0 = \frac{\partial}{\partial x_k} \left( d_{kij} \, \frac{1}{2} \left[ \frac{\partial \tilde{u}_i}{\partial x_j} + \frac{\partial \tilde{u}_j}{\partial x_i} \right] - \varepsilon_{kj} \, \frac{\partial \tilde{\varphi}}{\partial x_j} \right). \tag{1.15}$$

Initial conditions, Dirichlet boundary conditions and Neumann boundary conditions are added:

$$\begin{aligned} \tilde{u}_i(.,0) &= u_i, && x \in \Omega, \\ \tilde{u}_i &= 0, && i = 1,2,3, \quad x \in \Gamma_u, \\ \mathrm{T_{ij}} n_j &= f_i, && i = 1,2,3, \quad x \in \Gamma_f, \\ \tilde{\varphi}(.,0) &= \varphi, \\ \tilde{\varphi} &= \varphi_D, && x \in \Gamma_\varphi, \\ \mathrm{D_k} n_k &= q, && x \in \Gamma_q, \end{aligned} \tag{1.16}$$

where

$$\Gamma_u \cup \Gamma_f = \Gamma, \ \Gamma_u \cap \Gamma_f = \emptyset, \ \Gamma_\varphi \cup \Gamma_q = \Gamma, \ \Gamma_\varphi \cap \Gamma_q = \emptyset.$$

Right-hand side $f_i$ represents mechanical excitation by external mechanical forces, $q$ denotes electrical excitation by imposing surface charge (in the case of free oscillations, they are both zero).

Equations (1.14)-(1.15) define the problem of harmonic oscillation of the piezoelectric continuum under given conditions (1.16). We will discretize the problem using FEM. The discretization is the subject of the chapter 2.

## 1.4 Static deformation of piezoelectric continuum

The oscillation of the piezoelectric continuum is not the only problem solved in the area of piezoelectric materials. In addition to the problem (1.14)-(1.16) one can solve the static problem (not depending on time) of resonator loaded by constant electric field (actuating) or by constant outer forces (sensing),

$$\frac{\partial}{\partial x_j}\left(c_{ijkl}\,\frac{1}{2}\left[\frac{\partial u_k}{\partial x_l}+\frac{\partial u_l}{\partial x_k}\right]+d_{kij}\,\frac{\partial \varphi}{\partial x_k}\right)=0 \quad i=1,2,3, \tag{1.17}$$

$$\frac{\partial}{\partial x_k}\left(d_{kij}\,\frac{1}{2}\left[\frac{\partial u_i}{\partial x_j}+\frac{\partial u_j}{\partial x_i}\right]-\varepsilon_{kj}\,\frac{\partial \varphi}{\partial x_j}\right)=0, \tag{1.18}$$

$$\begin{aligned}
\tilde{u}_i &= \tilde{u}_{iD}, \quad i=1,2,3, \quad x\in\Gamma_u,\\
\mathrm{T_{ij}}n_j &= f_i, \quad i=1,2,3, \quad x\in\Gamma_f,\\
\tilde{\varphi} &= \varphi_D, \quad x\in\Gamma_\varphi,\\
\mathrm{D_k}n_k &= q, \quad x\in\Gamma_q.
\end{aligned}$$

This class of problems is solved, e.g., for actuators – piezoelectric devices, which react on changes of electric field. Problem (1.17)-(1.18) is special case of problem (1.14)-(1.16) and can be discretized in the same way.

# Chapter 2

# Weak formulation and discretization of the problem

Discretization of the problem (1.14)-(1.16) and the use of the finite element method is based on so called *weak formulation*. Its idea is following. Equations (1.14), resp. (1.15) represent energy, resp. electric flux conservation. These equations are elliptic partial differential equations and its exact solution must be an element of $C^{(2)}(\Omega) \cap C^{(0)}(\overline{\Omega})$. In fact, the requirements to the functions smoothness is too strong. Usually, the energy conservation laws are described with integral principles known from theoretical physic (see, e.g., [21]). So the idea is to transform equations (1.14), (1.15) "back" to the integral form, containing derivations of lower orders than in original equations. This process, described in next paragraph, is called weak formulation. Then we require the *weak solution* to fulfil integral equations in certain functional sense.

The other possible process, resulting in integral equalities, is use of the variational formulation and the Hamilton principle of energy conservation (see [1]).

## 2.1 Weak formulation

### 2.1.1 Functional spaces

We briefly sketch the functional spaces used in our weak formulation. We deal with the weak formulation derived in [16], chapters 28-35. For more details we recommend the reader to this book. We consider bounded domain $\Omega$ with Lipschitzian boundary $\Gamma$. Let $L_2(\Omega)$ be the Lebesgeue space of functions square integrable in $\Omega$, $\int_\Omega |f|^2 < +\infty$, with scalar product $(f,g)_\Omega = \int_\Omega f g d\Omega$. Further, let $C^{(\infty)}(\overline{\Omega})$ be functions, which, including derivatives of all orders, are continuous in $\overline{\Omega}$. The subspace $C_0^{(\infty)}(\overline{\Omega}) \subset C^{(\infty)}(\overline{\Omega})$ contains the functions with compact support. If for a function $u \in L_2(\Omega)$ exists some function $u^i \in L_2(\Omega)$, for which holds the integral equality

$$\int_\Omega u^i \psi d\Omega = -\int_\Omega u \frac{\partial \psi}{\partial x_i} d\Omega \quad \forall \psi \in C_0^{(\infty)}(\overline{\Omega}), \tag{2.1}$$

we call $u^i$ the *generalized derivative* of $u$ (for function from $C^{(\infty)}(\overline{\Omega})$, its generalized derivative equals to its classical derivative). *Sobolev space* $W_2^{(1)}(\Omega)$ is made of functions from $L_2(\Omega)$, which have generalized derivatives square integrable in $\Omega$.

To express values of function $u \in W_2^{(1)}(\Omega)$ on the boundary $\Gamma$, the *trace* of function $u$ is established (see [16]; for function from $C^{(\infty)}(\overline{\Omega})$, its trace is determined by its values on the boundary).

Now, we establish

$$V(\Omega) = \{v | v \in W_2^{(1)}(\Omega), \quad v|_{\Gamma_1} = 0 \text{ in the sense of traces}\},$$

the subspace of $W_2^{(1)}(\Omega)$, made of functions, which traces fulfil the homogenous boundary conditions.

### 2.1.2 Integral equalities

We will discretize the problem in spatial variables. We derive the weak formulation in the standard way ([16], chapter 31). We multiply the equations (1.14) with testing functions $w_i \in V(\Omega)$, summarize and integrate them over $\Omega$. As well, we multiply the equation (1.15) with testing function $\phi \in V(\Omega)$ and integrate it over $\Omega$. Using Green formula, we obtain the integral equalities (boundary integrals are denoted with sharp brackets)

$$\begin{aligned}\left(\varrho\frac{\partial^2\tilde{u}_i}{\partial t^2}, w_i\right)_\Omega + \left(c_{ijkl}\,\frac{1}{2}\left[\frac{\partial\tilde{u}_k}{\partial x_l} + \frac{\partial\tilde{u}_l}{\partial x_k}\right], \frac{\partial w_i}{\partial x_j}\right)_\Omega \\ + \left(d_{kij}\,\frac{\partial\tilde{\varphi}}{\partial x_k}, \frac{\partial w_i}{\partial x_j}\right)_\Omega = \left\langle f_i, w_i\right\rangle_{\Gamma_f},\end{aligned} \tag{2.2}$$

$$\left(d_{jik}\,\frac{1}{2}\left[\frac{\partial\tilde{u}_i}{\partial x_k} + \frac{\partial\tilde{u}_k}{\partial x_i}\right], \frac{\partial\phi}{\partial x_j}\right)_\Omega - \left(\varepsilon_{ji}\,\frac{\partial\tilde{\varphi}}{\partial x_i}, \frac{\partial\phi}{\partial x_j}\right)_\Omega = \left\langle q, \phi\right\rangle_{\Gamma_q}. \tag{2.3}$$

Due to the symmetry of material tensors, equations (2.2) and (2.3) are equivalent to

$$\begin{aligned}\left(\varrho\frac{\partial^2\tilde{u}_i}{\partial t^2}, w_i\right)_\Omega + \left(c_{ijkl}\,\frac{1}{2}\left[\frac{\partial\tilde{u}_k}{\partial x_l} + \frac{\partial\tilde{u}_l}{\partial x_k}\right], \frac{1}{2}\left[\frac{\partial w_i}{\partial x_j} + \frac{\partial w_j}{\partial x_i}\right]\right)_\Omega \\ + \left(d_{kij}\,\frac{\partial\tilde{\varphi}}{\partial x_k}, \frac{1}{2}\left[\frac{\partial w_i}{\partial x_j} + \frac{\partial w_j}{\partial x_i}\right]\right)_\Omega = \left\langle f_i, w_i\right\rangle_{\Gamma_f},\end{aligned} \tag{2.4}$$

$$\left(d_{jik}\,\frac{1}{2}\left[\frac{\partial\tilde{u}_i}{\partial x_k} + \frac{\partial\tilde{u}_k}{\partial x_i}\right], \frac{\partial\phi}{\partial x_j}\right)_\Omega - \left(\varepsilon_{ji}\,\frac{\partial\tilde{\varphi}}{\partial x_i}, \frac{\partial\phi}{\partial x_j}\right)_\Omega = \left\langle q, \phi\right\rangle_{\Gamma_q}. \tag{2.5}$$

Let us denote

$$\mathrm{R}_{ij} = \frac{1}{2}\left[\frac{\partial w_i}{\partial x_j} + \frac{\partial w_j}{\partial x_i}\right], \qquad i, j = 1, 2, 3.$$

Substituting these terms into equalities (2.4) and (2.5) gives simplified forms of integral equalities,

$$\left(\varrho\frac{\partial^2\tilde{u}_i}{\partial t^2}, w_i\right)_\Omega + (c_{ijkl}\,\mathrm{S}_{kl}, \mathrm{R}_{ij})_\Omega + \left(d_{kij}\,\frac{\partial\tilde{\varphi}}{\partial x_k}, \mathrm{R}_{ij}\right)_\Omega = \left\langle f_i, w_i\right\rangle_{\Gamma_f}, \tag{2.6}$$

$$\left(d_{jik}\,\mathrm{S}_{ik}, \frac{\partial\phi}{\partial x_j}\right)_\Omega - \left(\varepsilon_{ji}\,\frac{\partial\tilde{\varphi}}{\partial x_i}, \frac{\partial\phi}{\partial x_j}\right)_\Omega = \left\langle q, \phi\right\rangle_{\Gamma_q}. \tag{2.7}$$

**Weak solution.** Let

$$\tilde{\mathbf{u}}_D \in ([W_2^{(1)}(\Omega)]^3, C^{(2)}(0,\mathrm{T})),\ \tilde{\varphi}_D \in (W_2^{(1)}(\Omega), AC(0,\mathrm{T}))$$

satisfy the Dirichlet boundary conditions (in the weak sence). Further, let

$$\tilde{\mathbf{u}}_0 \in ([W_2^{(1)}(\Omega)]^3, C^{(2)}(0,\mathrm{T})),\ \varphi_0 \in (W_2^{(1)}(\Omega), AC(0,\mathrm{T}))$$

be functions, for which equalities (2.6) and (2.7) are observed for all choices of testing functions

$$\mathbf{w} = (w_1, w_2, w_3) \in [V(\Omega)]^3,\ \phi \in V(\Omega).$$

Then we define the *weak solution* of the problem (1.14)-(1.16) as

$$\tilde{\mathbf{u}} = \tilde{\mathbf{u}}_D + \tilde{\mathbf{u}}_0, \quad \tilde{\varphi} = \tilde{\varphi}_D + \tilde{\varphi}_0.$$

Weak solution, on the contrary to the classical solution, does not necessarily have continuous spatial derivatives of the 2nd order.The weak solution has generalized spatial derivatives (2.1) and satisfies the integral identities (2.6), (2.7).

## 2.2 Discretization of the problem

Finite element method constructs the finite dimensional approximation of the weak solution. The domain $\Omega$ is decomposed into a set of *finite elements*, where special basis functions are established. Then, weak solution as the linear combination of these basis functions is looked for. The parts $\mathbf{u}_D, \varphi_D$ of the weak solution, satisfying the Dirichlet boundary conditions, can be explicitly expressed in the linear system, resulting from discretization of the problem (2.6), (2.7), and are introduced in the Paragraph 2.3.

In our case, we use the following FEM approximation. In two steps, we decompose the domain $\Omega$ (which is the volume of the resonator) into the finite set $E^h$ of disjoint tetrahedral elements (the first step - shown in the Fig. 2.1 - means the division into the layers and prismatic elements, the second part the division of the prismatic elements into the tetrahedrons - Fig. 2.2). The domain $\Omega$ is approximated by the union of these tetrahedrons,

$$\Omega \sim \Omega^h = \bigcup_{e\in E^h} e, \quad \bigcup_{e\in E^h} e = \overline{\Omega},$$

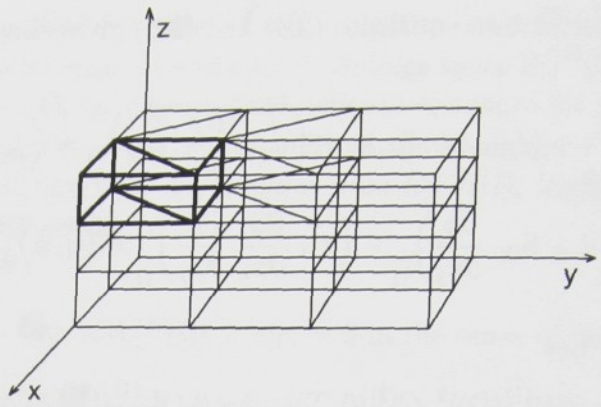


Figure 2.1: Division of a cubic crystal into layers and prismatic elements

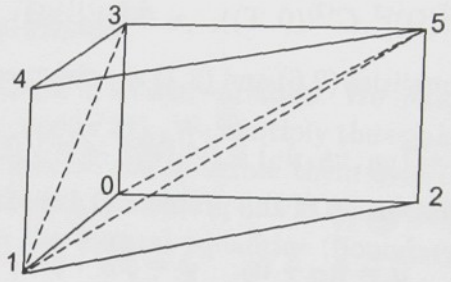


Figure 2.2: Division of a prismatic element into three tetrahedrons 0125, 0153 and 1534

where $h$ denotes the discretization parameter ($diam(e) < h \ \forall e \in E^h$). The boundary $\Gamma$ is approximated as

$$\Gamma^h = \partial\Omega^h.$$

On the union $\Omega^h$, we construct the finite dimensional approximation $V^h(\Omega)$ of the function space $V(\Omega)$. Functions from $V^h(\Omega)$ are piecewise linear and continuous on $\Omega^h$ and are zero on the boundary. For each element $e \in E^h$, we define set $\Psi^h(e)$ of four basis functions,

$$\Psi^h(e) = \{\psi_i^e(x, y, z) | i = 1, 2, 3, 4\},$$

For tetrahedrons, we choose the basis functions to be the linear multinominals,

$$\psi_i^e(x, y, z) = \alpha_{0i}^e + \alpha_{1i}^e x + \alpha_{2i}^e y + \alpha_{3i}^e z. \tag{2.8}$$

Consider an element $e = \{s^1, s^2, s^3, s^4\}$. Its $j$-th node $s^j$ has coordinates $(x_j, y_j, z_j)$. Basis functions can be uniquely defined by its values at the nodes $s^j$ of the element and have to satisfy

$$\psi_i^e(s^j) = \delta_{ij}, \qquad i, j = 1, 2, 3, 4.$$
$$\psi_i^e|_{\Omega^h - e} = 0, \qquad i = 1, 2, 3, 4.$$

The coefficients $\alpha_{,i}$ in (2.8) can be computed by inverting the matrix of node's coordinates:

$$\begin{pmatrix} 1 & x_1 & y_1 & z_1 \\ 1 & x_2 & y_2 & z_2 \\ 1 & x_3 & y_3 & z_3 \\ 1 & x_4 & y_4 & z_4 \end{pmatrix}^{-1} = \begin{pmatrix} \alpha^e_{01} & \alpha^e_{02} & \alpha^e_{03} & \alpha^e_{04} \\ \alpha^e_{11} & \alpha^e_{12} & \alpha^e_{13} & \alpha^e_{14} \\ \alpha^e_{21} & \alpha^e_{22} & \alpha^e_{23} & \alpha^e_{24} \\ \alpha^e_{31} & \alpha^e_{32} & \alpha^e_{33} & \alpha^e_{34} \end{pmatrix}$$

For each tetrahedron, the basis is made of four these linear multinominals. They generate the functional space $V^h(e)$,

$$V^h(e) = \{\psi^h | supp(\psi^h) \subset e, \quad \psi^h \in W_2^1(e), \quad \psi^h|_{\Omega - e} = 0\}.$$

The union

$$\Psi^h(\Omega) = \bigcup_{e \in E^h} \Psi^h(e)$$

forms the basis of function space

$$V^h(\Omega) = \bigcup_{e \in E^h} V^h(e),$$

which is the finite dimensional approximation of the space $V(\Omega)$[1]. The global approximations of the electric potential and displacement, lying in the space $V^h(\Omega)$, are:

$$\tilde{u}^h_i(\mathbf{x}) = \sum_{\psi^h_j \in \Phi^h} u^j_i(t)\psi^h_j(\mathbf{x}), \quad u^j_i : (0, \mathrm{T}) \to \mathbf{R}, \quad \mathbf{x} \in \Omega, \quad i = 1, 2, 3, \quad (2.9)$$

$$\tilde{\varphi}^h(\mathbf{x}) = \sum_{\psi^h_j \in \Phi^h} \varphi^j(t)\psi^h_j(\mathbf{x}), \quad \varphi^j : (0, \mathrm{T}) \to \mathbf{R}, \quad \mathbf{x} \in \Omega,$$

and for its derivatives holds

$$\frac{\partial \tilde{u}^h_i}{\partial x_i}(\mathbf{x}) = \sum_{\psi^h_j \in \Phi^h} u^j_i(t)\frac{\partial \psi^h_j}{\partial x_i}(\mathbf{x}), \quad \frac{\tilde{\varphi}^h}{\partial x_i}(\mathbf{x}) = \sum_{\psi^h_j \in \Phi^h} \varphi^j(t)\frac{\partial \psi^h_j}{\partial x_i}(\mathbf{x}). \quad (2.10)$$

Let the nodes of the division and the global basis functions be numbered, $(\psi^h_1, ..., \psi^h_r)$. We denote

$$\mathrm{U}^{\mathrm{T}} = (u^1_1(t), u^1_2(t), u^1_3(t), u^2_1(t), u^2_2(t), u^2_3(t), ..., u^r_1(t), u^r_2(t), u^r_3(t)), \quad (2.11)$$

$$\Phi^{\mathrm{T}} = (\varphi^1_1(t), \varphi^1_2(t), \varphi^1_3(t), \varphi^2_1(t), \varphi^2_2(t), \varphi^2_3(t), ..., \varphi^r_1(t), \varphi^r_2(t), \varphi^r_3(t)). \quad (2.12)$$

U and $\Phi$ are values of displacement and electric potential at the nodes of the mesh in time $t$. The approximations (2.9) are piecewise linear on $\Omega^h$, approximations

[1]The basis functions defined on nearby elements, which belong to the same node $i$ of division, form together one global basis function for $i$-th node. This function is normalized to have value one in the node $i$.

of derivatives are piecewise constant (in the spatial variable). We substitute approximations (2.9) and (2.10) into integral equalities (2.6) and (2.7). We require to them to be fulfilled for all basis functions $\psi_s^h$, $s \in \hat{r}$,

$$\left(c_{ijkl}\ \mathrm{S}_{\mathrm{kl}}^{\mathrm{h}}, \mathrm{R}_{\mathrm{ij}}^{\mathrm{h}}\right)_{\Omega} + \left(\varrho \frac{\partial^2 \tilde{u}_i^h}{\partial t^2}, \psi_s^h\right)_{\Omega} + \left(d_{kij}\ \frac{\partial \tilde{\varphi}^h}{\partial x_k}, \mathrm{R}_{\mathrm{ij}}^{\mathrm{h}}\right)_{\Omega} = \left\langle f_i, \psi_s^h \right\rangle_{\Gamma_f}, \tag{2.13}$$

$$\left(d_{jik}\ \mathrm{S}_{ik}^{h}, \frac{\partial \psi_s^h}{\partial x_j}\right)_{\Omega} - \left(\varepsilon_{ji}\ \frac{\partial \tilde{\varphi}^h}{\partial x_i}, \frac{\partial \psi_s^h}{\partial x_j}\right)_{\Omega} = \left\langle q, \psi_s^h \right\rangle_{\Gamma_q}. \tag{2.14}$$

For harmonic oscillation, the system of ordinary differential equations for values of displacement and potential in the nodes of division results, having block structure

$$\mathbb{M}\ddot{\mathrm{U}} + \mathbb{K}\mathrm{U} + \mathbb{P}^{\mathrm{T}}\Phi = \mathrm{F}, \tag{2.15}$$

$$\mathbb{P}\mathrm{U} - \mathbb{E}\Phi = \mathrm{Q}. \tag{2.16}$$

The submatrix $\mathbb{K}$ is the *elastic* matrix. It has a block structure

$$\mathbb{K} = \begin{pmatrix} \mathbb{K}_{11} & \mathbb{K}_{12} & \dots & \mathbb{K}_{1r} \\ \mathbb{K}_{21} & \mathbb{K}_{22} & \dots & \mathbb{K}_{2r} \\ \dots & \dots & \dots & \dots \\ \dots & \dots & \dots & \dots \\ \dots & \dots & \dots & \dots \\ \dots & \dots & \dots & \dots \\ \mathbb{K}_{r1} & \mathbb{K}_{r2} & \dots & \mathbb{K}_{rr} \end{pmatrix}. \tag{2.17}$$

If we denote the deformation matrix $\mathbb{B}^p$ for the $p$-th basis function as

$$\mathbb{B}^p = \begin{pmatrix} \frac{\partial}{\partial x_1}\psi_p^h(\mathbf{x}) & 0 & 0 \\ 0 & \frac{\partial}{\partial x_2}\psi_p^h(\mathbf{x}) & 0 \\ 0 & 0 & \frac{\partial}{\partial x_3}\psi_p^h(\mathbf{x}) \\ 0 & \frac{1}{2}\frac{\partial}{\partial x_3}\psi_p^h(\mathbf{x}) & \frac{1}{2}\frac{\partial}{\partial x_2}\psi_p^h(\mathbf{x}) \\ \frac{1}{2}\frac{\partial}{\partial x_3}\psi_p^h(\mathbf{x}) & 0 & \frac{1}{2}\frac{\partial}{\partial x_1}\psi_p^h(\mathbf{x}) \\ \frac{1}{2}\frac{\partial}{\partial x_2}\psi_p^h(\mathbf{x}) & \frac{1}{2}\frac{\partial}{\partial x_1}\psi_p^h(\mathbf{x}) & 0 \end{pmatrix},$$

then, for $p, q \in \hat{r}$, it is

$$\mathbb{K}_{pq} = \int_{\Omega^h} [\mathbb{B}^q]^{\mathrm{T}} \mathbb{C} \mathbb{B}^p d\Omega, \quad \mathbb{K}_{pq} \in \mathcal{R}^{3,3},$$

where $\mathbb{C}$ is the matrix of elastic modules (1.5). The mass matrix $\mathbb{M}$ has the block structure

$$\mathbb{M} = \begin{pmatrix} \mathbb{M}_{11} & \mathbb{M}_{12} & \dots & \mathbb{M}_{1r} \\ \mathbb{M}_{21} & \mathbb{M}_{22} & \dots & \mathbb{M}_{2r} \\ \dots & \dots & \dots & \dots \\ \dots & \dots & \dots & \dots \\ \dots & \dots & \dots & \dots \\ \dots & \dots & \dots & \dots \\ \mathbb{M}_{r1} & \mathbb{M}_{r2} & \dots & \mathbb{M}_{rr} \end{pmatrix}, \tag{2.18}$$

and consists of diagonal submatrices $\mathbb{M}_{pq}$,

$$(\mathbb{M}_{pq})_{ii} = \int_{\Omega^h} \psi_p^h \psi_q^h d\Omega, \quad i = 1, 2, 3, \quad \mathbb{M}_{pq} \in \mathcal{R}^{3,3},$$

Piezoelectric part of the system matrix has the block structure

$$\mathbb{P} = \begin{pmatrix} \mathbb{P}_{11} & \mathbb{P}_{12} & \dots & \mathbb{P}_{1r} \\ \mathbb{P}_{21} & \mathbb{P}_{22} & \dots & \mathbb{P}_{2r} \\ \vdots & \vdots & s & \vdots \\ \vdots & \vdots & s & \vdots \\ \mathbb{P}_{r1} & \mathbb{P}_{r2} & \dots & \mathbb{P}_{rr} \end{pmatrix}, \tag{2.19}$$

where ($\mathbb{D}$ is the matrix of piezoelectric coefficients (1.6))

$$\mathbb{P}_{pq} = \int_{\Omega^h} [\mathbb{B}^q]^{\mathrm{T}} \mathbb{D} (\nabla \psi_p^h) d\Omega, \quad \mathbb{P}_{pq} \in \mathcal{R}^{3,1}.$$

The electric matrix is

$$\mathbb{E} = \begin{pmatrix} \mathbb{E}_{11} & \dots & \mathbb{E}_{1r} \\ \mathbb{E}_{21} & \dots & \mathbb{E}_{2r} \\ \vdots & & \vdots \\ \mathbb{E}_{r1} & \dots & \mathbb{E}_{rr} \end{pmatrix}, \tag{2.20}$$

where

$$\mathbb{E}_{pq} = \int_{\Omega^h} (\nabla \psi_q^h)^{\mathrm{T}} \mathcal{E} (\nabla \psi_p^h) d\Omega, \quad \mathbb{E}_{pq} \in \mathcal{R}.$$

$\mathcal{E}$ is the permittivity matrix (1.7). Matrices $\mathbb{K}, \mathbb{M}, \mathbb{E}$ are symmetric. Vectors F and Q represent the mechanical and electrical excitation, respectively. F are nodal forces, resp. Q nodal charges,

$$\mathrm{F} = \begin{pmatrix} \mathrm{F}_1 \\ \mathrm{F}_2 \\ \vdots \\ \mathrm{F}_r \end{pmatrix}, \tag{2.21}$$

where

$$\mathrm{F}_p^{\mathrm{T}} = \int_{\Gamma^h} (f_1, f_2, f_3) \psi_p^h d\Gamma, \quad \mathrm{F}_p \in \mathcal{R}^{3,1},$$

resp.

$$\mathrm{Q}^{\mathrm{T}} = (\mathrm{Q}_1, \dots, \mathrm{Q}_r),$$

where

$$\mathrm{Q}_p = \int_{\Gamma^h} q \psi_p^h d\Gamma, \quad \mathrm{Q}_p \in \mathcal{R}.$$

## 2.3 Boundary conditions

We deal with Dirichlet boundary conditions (1.16) for displacement and electric potential. The introduction of the boundary conditions is sketched on the Fig. 2.3. First case is the homogenous boundary condition[2] for displacement $\mathbf{u}$. Let there be in some nodes prescribed zero displacements (on the Fig.2.3 marked with gray color). Then proper columns of the matrix (marked with gray color) are multiplied by zeros and can be eliminated. So can be eliminated the prescribed variables from the vector of unknowns. Now, the number of equation is bigger than the number of unknowns, thus the rows (marked with gray color) belonging to the known variables can be eliminated. The resulting submatrices $\mathbb{K}$ and $\mathbb{M}$ are symmetric and positive definite (due to the positive definiteness of material tensors, see e.g. [11], chapter 20).

The similar situation occurs, when the zero electric potential is prescribed[3]. Proper columns and rows can be eliminated and submatrix $\mathbb{E}$ becomes positive definite.

In the case of nonhomogeneous Dirichlet boundary conditions for electric potential, there are some differences. The part of the vector with prescribed values is marked with the grid. The proper columns of the matrix are multiplied by prescribed values and the resulting vector can be set to the right-hand side of the linear system. The rows (marked with the grid) belonging to the known variables can be eliminated. Resulting matrix $\mathbb{E}$ is symmetric and positive definite. The linear system with different right-hand side results, with deflated matrix,

$$\hat{\mathbb{M}}\ddot{\mathrm{U}} + \hat{\mathbb{K}}\mathrm{U} + \hat{\mathbb{P}}^{\mathrm{T}}\Phi = \mathrm{F} + \mathrm{F}_{\varphi}, \tag{2.22}$$

$$\hat{\mathbb{P}}\mathrm{U} - \hat{\mathbb{E}}\Phi = \mathrm{Q} + \mathrm{Q}_{\varphi}. \tag{2.23}$$

$\mathrm{F}_{\varphi}$ represents generated electric force, $\mathrm{Q}_{\varphi}$ generated surface charge.

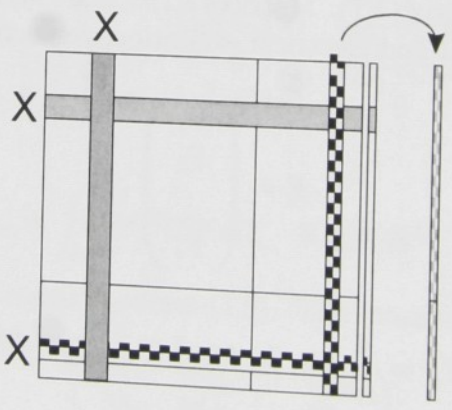


Figure 2.3: Introduction of boundary conditions into the linear system

[2]It is possible to prescribe here the nonhomogeneous displacement, but in practice, the zero displacement is established, e.g. due to resonator mounting.

[3]E.g. by the grounding of the resonator.

## 2.4 Input errors of the model

In the process of derivation of the model, we have made some simplifications on the physical reality. Further, we must deal with other errors resulting from the used methods.

We use the linear approximation $\mathbf{u}^h \in V^h(\Omega)$ of the weak solution $\mathbf{u} \in W_2^{(1)}(\Omega^h)$. The theory of approximation error is introduced e.g. in [3], we only mention here, that for our problem the global approximation estimate is proportional to $h$,

$$||\mathbf{u} - \mathbf{u}^h||_{W_2^{(1)}} \sim \mathcal{O}(h).$$

The same holds for approximation error for the weak solution of the potential $\varphi$.

Using the numerical integration of constant, linear or quadratic functions on the tetrahedral elements, we don't generate other error.

First simplification was made in establishing the piezoelectric equations of state. In the Hook's law, resp. Maxwell's equation, we used the linear dependance of the strain on the deformation - in the reality, this dependance is nonlinear and material tensors of higher orders must be used (see e.g. [27]), multiplied by the higher derivatives of displacement and potential. By this simplification, the error of order $\mathcal{O}(h^2)$ is generated, which is less then the error made by linear approximation in weak solution.

## 2.5 Dimension of the problem

The size of the matrices in (2.15) depends on the number of the nodes in the mesh, say $r$. From (2.17)-(2.20) can be seen that the sizes of the submatrices are

$$\mathbb{K}, \mathbb{M} \in \mathcal{R}^{3r,3r}, \ \mathbb{E} \in \mathcal{R}^{r,r}, \ \mathbb{P} \in \mathcal{R}^{r,3r}.$$

The submatrices are sparse. The blocks $\mathbb{K}_{pq}, \mathbb{M}_{pq}, \mathbb{E}_{pq}, \mathbb{P}_{pq}$ (according to the terms (2.17)-(2.20)), $p, q \in \hat{r}$, are nonzero only if $p = q$ or if nodes $s^p$ and $s^q$ have common edge. For our scheme of discretization, the number of nonzero blocks in each submatrix is proportional to $12r$ (in the worst case).

When Dirichlet boundary conditions are prescribed, the dimension of the submatrices decreases,

$$\hat{\mathbb{K}}, \hat{\mathbb{M}} \in \mathcal{R}^{3r_1,3r_1}, \ \hat{\mathbb{E}} \in \mathcal{R}^{r_2,r_2}, \ \hat{\mathbb{P}} \in \mathcal{R}^{r_2,3r_1},$$

where $r_1$ is number of the nodes, where no Dirichlet BC for the displacement are precribed, $r_2$ is number of the nodes with no prescribed Dirichlet BC for the potential.

# Chapter 3

# Points of interest

Let us write the system (2.22), (2.23) with introduced boundary conditions as

$$\mathbb{M}\ddot{\mathrm{U}} + \mathbb{K}\mathrm{U} + \mathbb{P}^{\mathrm{T}}\Phi = \tilde{\mathrm{F}}, \tag{3.1}$$

$$\mathbb{P}\mathrm{U} - \mathbb{E}\Phi = \tilde{\mathrm{Q}}, \tag{3.2}$$

where on the right-hand side are sums of external and generated forces and charges. The submatrices (here written without hats) have the properties described in Paragraph 2.3. This system describes the general oscillation of piezoelectric element, with mechanical or electrical excitation.

## 3.1 Free oscillation

The core of the behavior of the oscillating piezoelectric continuum lies in its free oscillation. Free oscillations (and computed eigenfrequencies) tells, when the system under external excitation can get to the resonance. There are two kinds of free oscillation of a piezoelectric system.

In the first type, electrodes are short-circuited, and for thin layers we can assume the electric potential to be zero in the whole volume ($\Phi = 0$). The problem reduces to the standard elastic oscillation case (compare with Paragraph 1.2),

$$\mathbb{M}\ddot{\mathrm{U}} + \mathbb{K}\mathrm{U} = 0.$$

Eigenfrequencies of the system can be found by solving the generalized eigenvalue problem,

$$(\mathbb{K} - \omega^2\mathbb{M})\mathrm{U} = 0.$$

Matrix $\mathbb{M}$ is positive definite (say of order $n$), so the problem has $n$ eigenvalues and eigenvectors as solution (see paragraph 1.2).

In the second type, the electrodes are open, i.e. external charges incoming to the electrodes are zero ($Q = 0$). Eigenfrequencies of the system can be found by solving the eigenvalue problem,

$$\begin{pmatrix} \mathbb{K} - \omega^2 \mathbb{M} & \mathbb{P}^{\mathrm{T}} \\ \mathbb{P} & -\mathbb{E} \end{pmatrix} \begin{pmatrix} \mathrm{U} \\ \Phi \end{pmatrix} = \begin{pmatrix} 0 \\ 0 \end{pmatrix}. \tag{3.3}$$

**Comment.** Sometimes, frequencies $\omega_1, ..., \omega_n$ from the first type of oscillation are called *resonance frequencies*. In resonance frequency, the system oscillates with minimal impedance. Eigenfrequencies of the second type are called *antiresonance frequencies*. In antiresonance frequency, the system oscillates with maximal impedance.

Widely used method in general oscillations of piezoelectric continuum is so called *static condensation*: substituting the potential from the second equation

$$\Phi = \mathbb{E}^{-1}(\mathbb{P}\mathrm{U} - \tilde{\mathrm{Q}}) \tag{3.4}$$

into the first equation to get one equation for the displacement,

$$\mathbb{M}\ddot{\mathrm{U}} + \mathbb{K}^{\star}\mathrm{U} = \tilde{\mathrm{F}} + \mathbb{P}^{\mathrm{T}}\mathbb{E}^{-1}\tilde{\mathrm{Q}},$$

where

$$\mathbb{K}^{\star} = \mathbb{K} - \mathbb{P}^{\mathrm{T}}\mathbb{E}^{-1}\mathbb{P}.$$

Static condensation gives

$$\mathbb{M}\ddot{\mathrm{U}} + \mathbb{K}^{\star}\mathrm{U} = 0.$$

The equation is similar to a pure elastic case, only elastic matrix $\mathbb{K}^{\star}$ contains the term representing the electromechanical coupling. Eigenfrequencies can be found by solving the eigenvalue problem

$$(\mathbb{K}^{\star} - \omega^2 \mathbb{M})\mathrm{U} = 0.$$

An other way is to solve the generalized eigenvalue problem

$$\mathbb{A}\mathrm{X} = \lambda \mathbb{B}\mathrm{X}$$

with

$$\mathbb{A} = \begin{pmatrix} \mathbb{K} & \mathbb{P}^{\mathrm{T}} \\ \mathbb{P} & -\mathbb{E} \end{pmatrix}$$

being symmetric and

$$\mathbb{B} = \begin{pmatrix} \mathbb{M} & 0 \\ 0 & 0 \end{pmatrix}$$

being symmetric and positive semidefinite matrix. This strategy is also possible for the case of proposed pure mechanical excitation of the vibration, when there are no prescribed Dirichlet boundary conditions for electric potential and the electric submatrix is therefore singular[4].

[4]We can only define the zero value of electric potential at least at one node of mesh to make the electric matrix $\mathbb{E}$ regular, e.g. by grounding a part of the resonator. In applications, a part of the resonator is usually grounded.

## 3.2 Damped oscillation

If we deal with the structural damping of the piezoelectric material, the first governing equation extends of the damping term (see e.g. [24]),

$$\mathbb{M}\ddot{\mathrm{U}} + \mathbb{H}\dot{\mathrm{U}} + \mathbb{K}\mathrm{U} + \mathbb{P}^{\mathrm{T}}\Phi = \mathrm{F},$$

where $\mathbb{H}$ is the structural damping matrix

$$\mathbb{H} = \alpha\mathbb{M} + \beta\mathbb{K}, \quad \alpha, \beta \in [0, 1], \quad \alpha + \beta = 1.$$

## 3.3 Static problem

For the static case, the problem reduces to solving the system of linear equations,

$$\begin{aligned} \mathbb{K}\mathrm{U} + \mathbb{P}^{\mathrm{T}}\Phi &= \mathrm{F}, \\ \mathbb{P}\mathrm{U} - \mathbb{E}\Phi &= \mathrm{Q}. \end{aligned} \tag{3.5}$$

It is the saddle point problem.

## 3.4 Controlled oscillation

The most general case is sketched on Fig. 3.1. It describes the smart plate consisting of two piezoelectric layers and one elastic layer in the middle (published e.g. in [24]). The elastic part is oscillating under the outer mechanical excitation (with force F). The voltage output, generated by the oscillation, is driven from the sensing layer to the amplifier and sent back to the actuating layer (charge Q). With proper amplifying, we want to control the oscillations of the system. Governing equations are [24]

$$\mathbb{M}\ddot{\mathrm{U}} + \mathbb{H}\dot{\mathrm{U}} + \mathbb{K}\mathrm{U} + \mathbb{P}^{\mathrm{T}}\Phi = \mathrm{F}, \tag{3.6}$$

$$\mathbb{P}\mathrm{U} - \mathbb{E}\Phi = \mathrm{Q}. \tag{3.7}$$

From (3.7) we have the sensor output,

$$\Phi = \mathbb{E}^{-1}(\mathbb{P}\mathrm{U} - \mathrm{Q}).$$

In the sensing layer, usually $\mathrm{Q} = 0$. The generated voltage is sent to the amplifier. Feedback voltage (charge) from the amplifier is chosen to oppose the current motion of the plate,

$$\mathrm{Q} = -G\dot{\Phi} = -G\ \mathbb{E}^{-1}\mathbb{P}\dot{\mathrm{U}},$$

where $G$ is the feedback gain. It is sent back to the actuating level. Substituting above terms in (3.7) and then in (3.6) gives motion equation,

$$\mathbb{M}\ddot{\mathrm{U}} + (\mathbb{H} + \mathbb{P}^{\mathrm{T}}\mathbb{E}^{-1}G\ \mathbb{E}^{-1}\mathbb{P})\dot{\mathrm{U}} + (\mathbb{K} - \mathbb{P}^{\mathrm{T}}\mathbb{E}^{-1}\mathbb{P})\mathrm{U} = \mathrm{F}. \tag{3.8}$$

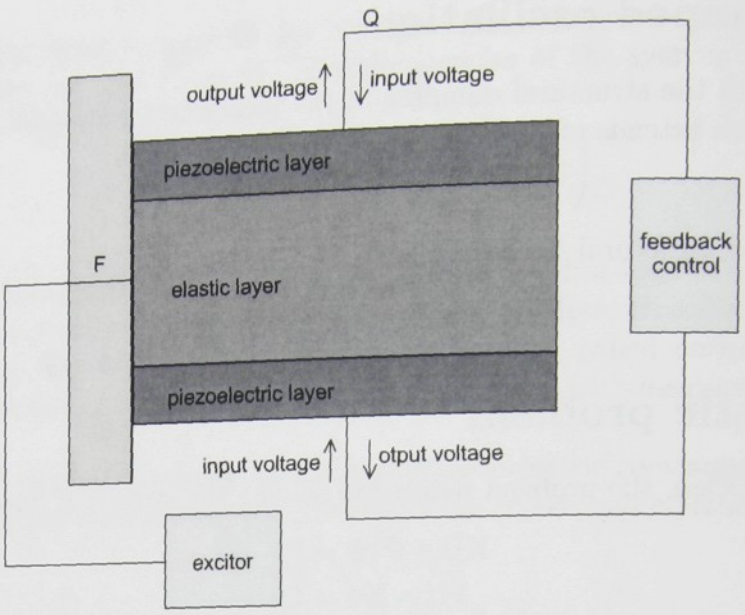


Figure 3.1: Scheme of composite plate with active control

## 3.5 Selection of dominant modes

In practice, one would produce resonators, where particular oscillation mode can be excited easily than the others. Such oscillation modes are called *dominant.*

### 3.5.1 Electromechanical coupling coefficients

The measure of excitation of particular mode can be expressed by its *electromechanical coupling coefficient* $k$, which is defined by the relation [10]

$$k^2 = \frac{E_m^2}{E_{st} E_d},$$

where

$$E_m = \frac{1}{2}\left(\mathrm{U}^T \mathbb{P} \Phi\right)$$

is the mutual energy,

$$E_{st} = \frac{1}{2}\left(\mathrm{U}^T \mathbb{K} \mathrm{U}\right)$$

is the elastic energy and

$$E_d = \frac{1}{2}\left(\Phi^T \mathbb{E} \Phi\right)$$

is the dielectric energy. The higher is the value of $k$, the better is the possibility of an excitation of the oscillation mode.

All computed eigenvalues and eigenvectors define the oscillation modes. They are sorted according to their electromechanical coupling coefficients and the modes with highest those coefficients can be easily found.

# Chapter 4

# Numerical methods for solving algebraic problems and their properties

There are two basic approaches to solve the eigenvalue problems. At first, we can solve the complete eigenvalue problem, which involves to transform the original problem to simpler forms and then compute all the eigenvalues (e.g. the QR algorithm which is looking for the Schur factorizations of the matrices). This approach is impossible (practically) for large eigenproblems due to its high memory costs.

When we are not interested in all eigenvalues, we can solve the partial eigenvalue problem, which means to find only several eigenvalues, that we are interested in. For this case, we can use Krylov subspace method.

## 4.1 Krylov subspace methods

We focus on methods which are suitable for solving large eigenproblems, especially on algorithms called *Krylov subspace projection methods* (KSM). Their idea is to look for an approximation of the eigenvector as linear combination of certain power sequence (successive vectors from power method), which, hopefully, may contain additional information not only about the eigenvector with largest magnitude (this does the power method), but also about the eigenvectors with other directions. Such linear combination form the *Krylov subspace*,

$$\mathcal{K}_k(\mathbb{A}, \mathbf{v}) = Span\{\mathbf{v}_1, \mathbb{A}\mathbf{v}_1, \mathbb{A}^2\mathbf{v}_1, ..., \mathbb{A}^{k-1}\mathbf{v}_1\}. \tag{4.1}$$

It is not suitable to use the explicit basis of the Krylov subspace from (4.1), because the vectors from the Krylov sequence become linearly dependent for increasing $k$.

Basis of Krylov subspace is usually formed by orthogonalizing the Krylov sequence (the power sequence above) by virtue of certain decomposition. They are called Arnoldi decompositions for non-Hermitian matrices and Lanczos decompositions for Hermitian matrices.

### 4.1.1 Arnoldi factorization

Arnoldi factorization builds the orthonormal basis of Krylov subspace. The relation

$$\mathbb{A}\mathbb{V}_k = \mathbb{V}_{k+1}\hat{\mathbb{H}}_k, \tag{4.2}$$

where $\mathbb{V}_k = (\mathbf{v}_1, \mathbf{v}_2, ..., \mathbf{v}_k) \in \mathcal{R}^{n\times(k+1)}$ has orthonormal columns and $\hat{\mathbb{H}}_k$ is unreduced upper Hessenberg matrix, is called *Arnoldi decomposition of order k* (if $\mathbb{H}$ is reduced, then we called the Arnoldi factorization *reduced*). For the detailed description of the algorithm for Arnoldi factorization, see e.g. [20] or [9].

Let us write upper Hessenberg matrix $\hat{\mathbb{H}}_k$ as

$$\hat{\mathbb{H}}_k = \begin{pmatrix} \mathbb{H}_k \\ \beta_k \mathbf{e}_k^{\mathrm{T}} \end{pmatrix}$$

Then Arnoldi decomposition (4.2) can be rewritten to

$$\mathbb{A}\mathbb{V}_k = \mathbb{V}_k\mathbb{H}_k + \beta_k \mathbf{v}_{k+1}\mathbf{e}_k^{\mathrm{T}}. \tag{4.3}$$

If we compute the eigenpair $(\lambda, \mathbf{s})$ of the matrix $\mathbb{H}_k$,

$$\mathbb{H}_k\mathbf{s} = \lambda\mathbf{s},$$

then for the vector $\mathbf{x} = \mathbb{V}_k\mathbf{s}$ the relation

$$\|\mathbb{A}\mathbf{x} - \lambda\mathbf{x}\| = \|(\mathbb{A}\mathbb{V}_k - \mathbb{V}_k\mathbb{H}_k)\mathbf{s}\| = |\beta_k \mathbf{e}_k^{\mathrm{T}}\mathbf{s}| \tag{4.4}$$

holds. The Ritz pair $(\lambda, \mathbf{x})$ is an approximate eigenpair of the matrix $\mathbb{A}$ and for $\mathbb{A}$ being Hermitian, the value (4.4) gives rigorous bound on the residual of the eigenvalues of $\mathbb{H}_k$ as approximations to eigenvalues of $\mathbb{A}$. As $k$ increases, some of these Ritz pairs will hopefully converge to the eigenpairs of $\mathbb{A}$.

**Comment - Arnoldi algorithm and eigenvalues. Theorem [23]**: As long the Arnoldi algorithm does not break down (i.e., $\mathcal{K}_n$ is of full rank $n$), the problem

$$\text{Find polynomial } p^n \in P^n \text{ such that } \|p^n(\mathbb{A})b\| = \text{minimum}.$$

has a unique solution, which is the characteristic polynomial of $\mathbb{H}_n$.

An effective means to get the polynomial $p^n$, for which $p^n(\mathbb{A})$ is small, is to take $p^n$ such that it has zeros close to the eigenvalues of $\mathbb{A}$. Due to the fact, that we do not compute the exact eigenvalues of $\mathbb{H}_n$, the resulting polynomial and eigenvalues of $\mathbb{A}$ are approximate.

The problem is, that we don't know, how many steps we need to get good approximation. On the other hand, the number of iterations of the Arnoldi algorithm is limited by the amount of computer memory to store $\mathbb{V}_k$. The fall-back can be to restart the Arnoldi process, when the $k$ becomes too large. There are more techniques to restart the Arnoldi method. We will use an implicit restarting.

### 4.1.2 Implicitly restarted Arnoldi algorithm

Let us suppose, that we are interested in first $k$ eigenpairs. The restarting is made trough the polynomial filtering of the starting vector. We want to damp the unwanted components and have the new starting vector lying in the $k$-dimensional invariant subspace (made of those Ritz vectors we are interested in). Implicit restarting continually compresses the interesting information into this subspace. The process uses the implicitly shifted QR algorithm.

**Polynomial filtering** Let us have matrix $\mathbb{A}$ with complete system of $n$ eigenpairs $(\lambda_i, \mathbf{x}_i)$ and suppose, that we are interested in first $k$ eigenpairs. Any vector $\mathbf{v}_1$ can be written as

$$\mathbf{v}_1 = \sum_{i=1}^{k} \gamma_i \mathbf{x}_i + \sum_{i=k+1}^{n} \gamma_i \mathbf{x}_i.$$

Then for any polynomial $\psi$ we have

$$\psi(\mathbb{A})\mathbf{v}_1 = \sum_{i=1}^{k} \gamma_i \psi(\lambda_i)\mathbf{x}_i + \sum_{i=k+1}^{n} \gamma_i \psi(\lambda_i)\mathbf{x}_i.$$

If $\psi$ is such, that values $\psi(\lambda_i)$ are large for $i = 1, ..., k$ and small for $i = k+1, ..., n$, we call $\psi$ the *filter polynomial.*

When we have computed (anyhow) the Ritz values $\mu_1, ..., \mu_m$ and we are not interested in the part of the spectrum corresponding to $\mu_{k+1}, ..., \mu_m$, we can take

$$\psi(t) = (t - \mu_{k+1})...(t - \mu_m).$$

**Implicit restarting** It is too expensive to use filter polynomial directly in the form written above, but we can easily compute the Krylov decomposition of application of the filter polynomial to the vector. This is the implicit restarting technique.

At first, we compute the Arnoldi factorization of length $m = k + p$,

$$\mathbb{A}\mathbb{V}_m = \mathbb{V}_m \mathbb{H}_m + \beta_m \mathbf{v}_{m+1} \mathbf{e}_m^{\mathrm{T}}, \tag{4.5}$$

where $m$ is chosen such large, that the decomposition can be stored in the memory. Then filter polynomial $\psi$ of order $p$ is chosen as

$$\psi(t) = (t - \kappa_1)...(t - \kappa_p)$$

and we use the implicit restarting to reduce the decomposition (4.5) of order $m$ to a decomposition of order $k$,

$$\mathbb{A}\widetilde{\mathbb{V}}_k = \widetilde{\mathbb{V}}_k \widetilde{\mathbb{H}}_k + \widetilde{\beta}_k \widetilde{\mathbf{v}}_{k+1} \mathbf{e}_k^{\mathrm{T}} \tag{4.6}$$

with starting vector $\psi(\mathbb{A})\mathbf{v}_1$. The shift $\kappa_1, ..., \kappa_p$ are selected as unwanted directions from the spectrum of matrix $\mathbb{H}_m$.

The above mentioned process is accomplished by the implicitly shifted QR algorithm. We can get the reduced decomposition (4.6) without explicitly using of filter polynomial.

Stepwise, for $j = 1, 2, ..., p$, we computed QR factorization of the shifted decomposition

$$(\mathbb{A} - \kappa_j \mathbb{I})\mathbb{V}_m = \mathbb{V}_m(\mathbb{H}_m - \kappa_j \mathbb{I}) + \beta_m \mathbf{v}_{m+1}\mathbf{e}_m^{\mathrm{T}},$$

which is

$$(\mathbb{A} - \kappa_j \mathbb{I})\mathbb{V}_m = \mathbb{V}_m \mathbb{Q}_j \mathbb{R}_j + \beta_m \mathbf{v}_{m+1}\mathbf{e}_m^{\mathrm{T}}.$$

After postmultiplying by $\mathbb{Q}_j$ we get

$$(\mathbb{A} - \kappa_j \mathbb{I})(\mathbb{V}_m \mathbb{Q}_j) = (\mathbb{V}_m \mathbb{Q}_j)(\mathbb{R}_j \mathbb{Q}_j) + \beta_m \mathbf{v}_{m+1}(\mathbf{e}_m^{\mathrm{T}} \mathbb{Q}_j).$$

If we denote

$$\mathbb{V}_m^{(j)} = \mathbb{V}_m \mathbb{Q}_j, \qquad \mathbb{H}_m^{(j)} = \mathbb{R}_j \mathbb{Q}_j + \kappa_j \mathbb{I}, \qquad \mathbf{b}_{m+1}^{(j)\mathrm{T}} = \mathbf{e}_m^{\mathrm{T}} \mathbb{Q}_j,$$

we finally have

$$\mathbb{A}\mathbb{V}_m^{(j)} = \mathbb{V}_m^{(j)} \mathbb{H}_m^{(j)} + \beta_m \mathbf{v}_{m+1} \mathbf{b}_{m+1}^{(j)\mathrm{T}}.$$

Accomplishing all the steps results in

$$\mathbb{A}\mathbb{V}_m^{+} = \mathbb{V}_m^{+} \mathbb{H}_m^{+} + \beta_m \mathbf{v}_{m+1} \mathbf{b}_{m+1}^{+\mathrm{T}},$$

where

$$\mathbb{V}_m^{+} = \mathbb{V}_m \mathbb{Q}, \quad \mathbb{H}_m^{+} = \mathbb{Q}^{\mathrm{T}} \mathbb{H}_m \mathbb{Q}, \quad \mathbb{Q} = \mathbb{Q}_1 ... \mathbb{Q}_p.$$

First $k$ columns of this decomposition can be written as

$$\mathbb{A}\widetilde{\mathbb{V}}_k = \widetilde{\mathbb{V}}_k \widetilde{\mathbb{H}}_k + \widetilde{\beta}_k \widetilde{\mathbf{v}}_{k+1} \mathbf{e}_k^{\mathrm{T}},$$

where

$$\widetilde{\beta}_k = \| h_{k+1,k} \mathbf{v}_{k+1}^{+} + \beta_k q_{m,k} \mathbf{v}_{m+1} \|_2, \quad \mathbf{v}_{k+1}^{+} = \widetilde{\beta}_k^{-1} (h_{k+1,k} \mathbf{v}_{k+1}^{+} + \beta_k q_{m,k} \mathbf{v}_{m+1}).$$

$\widetilde{\mathbb{H}}_k$ is the leading submatrix of $\mathbb{H}_m^{+}$ and $\widetilde{\mathbb{V}}_k$ consists of first $k$ columns of $\mathbb{V}_m^{+}$.

This is nothing less then the $k$-order Arnoldi decomposition with starting vector being proportional to $(\mathbb{A} - \kappa_1 \mathbb{I})...(\mathbb{A} - \kappa_p \mathbb{I})$, e.g. the starting vector was filtered by $\psi(\mathbb{A})$. So we get the reduced decomposition (4.6).

## 4.2 Generalized eigenvalue problem

In former chapters, we have transformed the problem of finding the resonance frequencies to solving the generalized eigenvalue problem

$$\mathbb{A}\mathrm{X} = \lambda \mathbb{B}\mathrm{X}, \tag{4.7}$$

where, in general,

$$\mathbb{A} = \begin{pmatrix} \mathbb{K} & \mathbb{P}^{\mathrm{T}} \\ \mathbb{P} & -\mathbb{E} \end{pmatrix}, \qquad \mathbb{B} = \begin{pmatrix} \mathbb{M} & 0 \\ 0 & 0 \end{pmatrix}, \qquad \mathrm{X} = \begin{pmatrix} \mathrm{U} \\ \Phi \end{pmatrix}, \tag{4.8}$$

with positive semi-definite matrix $\mathbb{B}$ or, by using static condensation,

$$\mathbb{A} = \mathbb{K} - \mathbb{P}^{\mathrm{T}}\mathbb{E}^{-1}\mathbb{P}, \qquad \mathbb{B} = \mathbb{M}, \qquad \mathrm{X} = \mathrm{U}, \tag{4.9}$$

with positive definite matrix $\mathbb{B}$.

### 4.2.1 B-Arnoldi method

For the generalized eigenvalue problem, a modification of the Arnoldi method can be used. Using a shift $\kappa$, the equation

$$\mathbb{A}\mathrm{X} = \lambda\mathbb{B}\mathrm{X}$$

is equivalent to

$$(\mathbb{A} - \kappa\mathbb{B})\mathrm{X} = (\lambda - \kappa)\mathbb{B}\mathrm{X}$$

and we can write

$$(\mathbb{A} - \kappa\mathbb{B})^{-1}\mathbb{B}\mathrm{X} = (\lambda - \kappa)^{-1}\mathrm{X}.$$

If we set

$$\mathbb{C} = (\mathbb{A} - \kappa\mathbb{B})^{-1}\mathbb{B}, \quad \mu = (\lambda - \kappa)^{-1},$$

we obtain the ordinary eigenproblem

$$\mathbb{C}\mathrm{X} = \mu\mathrm{X}.$$

Matrix $\mathbb{C}$ is called the *generalized shift-and-invert transform.*

During the Arnoldi process, we must compute the product $\mathbf{v} = \mathbb{C}\mathbf{u}$. This can be accomplished in two steps,

1. $\mathbf{w} = \mathbb{C}\mathbf{u}$
2. *solve* $(\mathbb{A} - \kappa\mathbb{B})\mathbf{v} = \mathbf{w}$

Thus we have to provide (somehow) solving of the linear system in step 2.

**$\mathbb{B}$-inner product** For positive definite matrix $\mathbb{B}$, the $\mathbb{B}$-inner product is defined by

$$(\mathbf{x}, \mathbf{y})_{\mathbb{B}} = \mathbf{y}^{\mathrm{T}}\mathbb{B}\mathbf{x}.$$

$\mathbb{B}$-norm or $\mathbb{B}$-orthogonality are defined as usual, using the $\mathbb{B}$-inner product.

The B-Arnoldi method computes the Arnoldi decomposition

$$\mathbb{C}\mathbb{V}_k = \mathbb{V}_k\mathbb{H}_k + \beta_k\mathbf{v}_{k+1}\mathbf{e}_k^{\mathrm{T}},$$

where $U_k$ is now $\mathbb{B}$-orthonormal. The implicitly restarting technique can be used without any changes.

Although we have defined the $\mathbb{B}$-inner product for positive definite matrix $\mathbb{B}$, we can apply the above algorithm also for $\mathbb{B}$ being positive semi-definite (now we use the semi-inner product instead of inner product). The possible problems can be caused by the fact, that this semi-inner product does not recognize the vectors lying in the null space of the matrix $\mathbb{B}$. Potentially, the error in direction lying in the null space of $\mathbb{B}$ can increase.[5]

## 4.3 Comments - reducing size of algebraic problem

### 4.3.1 Necessity to have large matrices

As was mentioned before in this chapter, the area of practicability of the numerical methods is restricted mostly by the amount of computer memory. Therefore, we cannot use too large matrices (that is why we use implicit restart).

Towards this argument stays the need of mesh being as fine as possible, to obtain good approximation of the weak solution. Moreover, not every oscillation mode can be expressed by the use of arbitrary mesh. The mathematical model itself behaves as frequency filter - it is able to compute only some frequencies and corresponding oscillation modes, depending up the fineness of the mesh. Particular mode with very complicated shape can be approximated with linear (base) functions only for very dense distribution of nodes and elements. This problem is not described for general case, but in practice this strategy seems to be satisfactory [4]: when we want to compute some particular oscillation mode, we have to use 3 elements for its wavelength.

For computation of complicated mode, we need to have the mesh, which is fine enough to catch the shape of the mode. Therefore we look for other ways to decrease size of used matrices.

### 4.3.2 Using static condensation

One of them already introduced is the static condensation. For the generalized eigenvalue problem (4.7) with matrices defined by case (4.9), the matrix $\mathbb{B}$ is symmetric and positive definite, and the problem can be transformed to the standard eigenvalue problem trough the Choleski factorization of matrix $\mathbb{M}$,

$$\mathbb{M} = \mathbb{L}\mathbb{L}^{\mathrm{T}}.$$

Then eigenvalues for the matrix pencil $(\mathbb{A}, \mathbb{M})$ are the same as for matrix $\widehat{\mathbb{A}} = \mathbb{L}^{-1}\mathbb{A}\mathbb{L}^{-\mathrm{T}}$ and the eigenvectors can be computed by solving $\mathbb{L}^{\mathrm{T}}\mathbf{x} = \widehat{\mathbf{x}}$, where $\widehat{x}$ is an

[5] For the problem (4.8), the null space directions are those which belong to electric potential $\Phi$, whereas the components of displacement U stay unharmed.

eigenvector of $\widehat{\mathbb{A}}$ (see paragraph 1.2). Implementation of factorization methods are available e.g. in Lapack library [32]. This approach we used in [37].

The dimension of the problem decreased to $3r_1$ (see paragraph 2.5). But - in the process of static condensation (3.4), we lost the sparseness of matrix $\mathbb{A}$ due to the inverting of matrix $\mathbb{E}$. During the IRA process we deal with still symmetric, but dense matrix, not much smaller than the original one (and have to solve the linear system with this matrix in each IRA step). Following numerical experiments and arguments in the last paragraph (in our case, we can use the B-Arnoldi method for original matrix pencil), we stay loyal to the original eigenproblem (4.8).

### 4.3.3 Reducing the oscillation to some direction

One way to decrease the dimension of the problem can be used, when we are interested in the oscillation in particular direction or in some plane. Then we can easily reduce the size of the eigenproblem.

Let us imagine a model example of an oscillating system, whose eigenfrequencies are found by solving of the generalized eigenvalue problem

$$\mathbb{A}X = \mathbb{M}X.$$

It involves information of general spatial oscillation modes. Let's say, that we want to find particular oscillation mode in only one direction (e.g. in the case of longitudinal oscillation). So, let this problem have the eigenpair $(\lambda, \mathrm{U})$, where the eigenvector has nonzero components in one direction and zero (or considerably small) components corresponding to other directions. Without a detriment to commonness, let the eigenvector have a structure $\mathrm{U} = (\mathrm{U}_1, 0)^{\mathrm{T}}$. The eigenpair satisfies the relation

$$\begin{pmatrix} \mathrm{A}_{11} & \mathrm{A}_{12}^{\mathrm{T}} \\ \mathrm{A}_{12} & \mathrm{A}_{22} \end{pmatrix} \begin{pmatrix} \mathrm{U}_1 \\ 0 \end{pmatrix} = \lambda \begin{pmatrix} \mathrm{M}_{11} & \mathrm{M}_{12}^{\mathrm{T}} \\ \mathrm{M}_{12} & \mathrm{M}_{22} \end{pmatrix} \begin{pmatrix} \mathrm{U}_1 \\ 0 \end{pmatrix},$$

and therefore $(\lambda, \mathrm{U}_1)$ must be also the eigenpair of the smaller problem

$$\mathrm{A}_{11}X = \lambda \mathrm{M}_{11}X.$$

We can solve the smaller problem, and if its solution $(\lambda, \mathrm{U})$ satisfies (at least approximately) $\mathrm{A}_{12}\mathrm{U} = \lambda \mathrm{M}_{12}\mathrm{U}$, then $(\lambda, (\mathrm{U}, 0)^{\mathrm{T}})$ is the solution of the original problem.

Many basic oscillation modes are restricted to one direction or to one plane, so we can use the spatial reduction in many occasions. As follows, e.g. for one dimensional oscillation modes, we can decrease the dimension of the problem to one half.

# Chapter 5

# Computer implementation of the model

The realization of the model consists of three parts: preprocessing, processing and postprocessing (Fig. 5.2). The pre- and postprocessing parts include use of the free

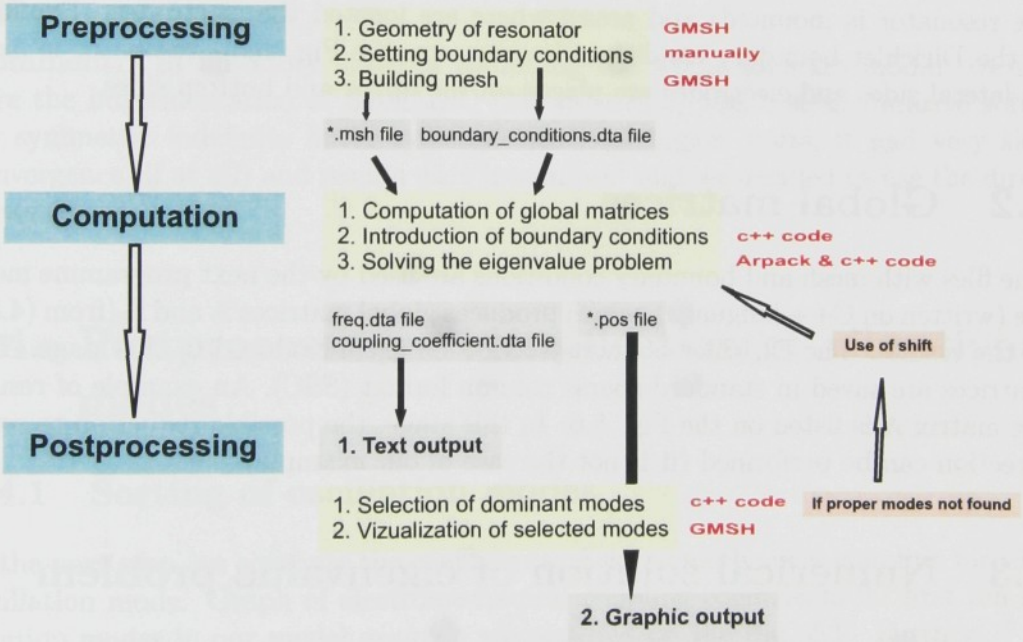


Figure 5.2: Scheme of computer implementation of the model and its stages.

software GMSH [33] for mesh generation and visualization of the results. For building the global matrices, we developed our own code written in C++ language. For solving the generalized eigenvalue problem, we use the Arpack [28] implementation of implicitly shifted Arnoldi method (in Fortran code), which is completed with our C++ code. All parts are debugged under Windows XP.

## 5.1 Preprocessing - geometry and mesh

GMSH software allows to make the three dimensional mesh of the users like geometry [34]. The geometry is made by defining points, oriented lines, oriented surfaces and volumes. Compound groups of geometrical entities can be defined, based on these elementary geometric entities. By the particular components, we can build the whole geometry of the resonator. An example of the geometry is shown on the Fig. 5.3 (beam resonator). Information of the geometry is stored in the $*.geo$ file. The geometry file corresponding to the defined geometry is shown below on the Fig. 5.3. Component $h$ is the discretization parameter.

The mesh consists of elementary geometrical elements of various shapes (in Gmshs case: lines, triangles, quadrangles, tetrahedra, prisms, hexahedra and pyramids), arranged in such a way that if two of them intersect, they do so along a face, an edge or a node, and never otherwise [34]. The mesh is unstructured. We use tetrahedral elements. Information of the mesh is stored in the $*.msh$ file. The mesh and corresponding mesh file are shown on the Fig. 5.4. All the other examples in this chapter use this mesh. Dirichlet boundary condition are prescribed per text file *diskr.par*. We specify the geometrical entities with zero displacement (where the resonator is mounted) and areas, where are located the electrodes. Example of the Dirichlet boundary conditions is shown on the Fig. 5.5 - resonator is fixed on lateral sides and electrodes are placed on the upper and bottom sides.

## 5.2 Global matrices

The files with mesh and boundary conditions are used by the next programme module (written on C++ language), which produces global matrices $\mathbb{A}$ and $\mathbb{B}$ (from (4.8)) as the results. The Dirichlet boundary condition are introduced in this stage. The matrices are saved in standard sparse column format (SSC). An example of resulting matrix $\mathbb{A}$ is listed on the Fig. 5.6. In this stage, the possible reduction to some direction can be performed (it is not the case of our example).

## 5.3 Numerical solution of eigenvalue problem

The algebraic modules work with matrix files described above.

### 5.3.1 ARPACK

ARPACK [28] module is an implementation of implicitly shifted Arnoldi algorithm. It is written in Fortran language. Application of the ARPACK procedures is described in the handbook [9]. It allows to use several computation routine for generalized eigenvalue problem, which differ in used mode of shift invert transform

of the matrix pencil (see Paragraph 4.2.1). We use the shift invert mode[6] for generalized eigenvalue problem in double precision (the *DSAUPD routine, see [9]*).

Parameters needed for computation are transmitted trough the file *geneig.par* (see upper part of Fig. 5.7). Resulting Ritz pairs (approximate eigenvalues and eigenvectors) are described on the Fig. 5.8.

### 5.3.2 SKYPACK

As we have mentioned in paragraph 4.2.1, in each IRA step we have to provide solving of linear system with sparse symmetric indefinite matrix. We use the SKYPACK [31] module. It is the direct solver for symmetric indefinite linear systems. It requires the upper triangle of matrices $\mathbb{A}$ and $\mathbb{B}$, stored in so called *skyline form*. Then it provides the $\mathbb{LDL}^T$ factorization of the matrix pencil $(\mathbb{A} - \kappa\mathbb{B})$ (see Paragraph 4.2.1) and solution of the system $(\mathbb{A} - \kappa\mathbb{B})\mathbf{v} = \mathbf{w}$ during the IRA step. For detailed description of the computational routines and about the skyline form of the matrix, see [30].

**Comment.** In initiatory stage of compiling the whole software modul, we use here the implementation of SYMMLQ [29] algorithm, which is an iterative solver for symmetric indefinite linear systems. But, for bigger shifts, it had very slow convergence (if at all) and results were inaccurate[7] and we decided to use the direct solver instead.

## 5.4 Postprocessing - identification of vibrational modes

### 5.4.1 Sorting of oscillation modes

In the next step, we compute the coefficients of electromechanical coupling for each oscillation mode. Graph of electromechanical coupling coefficients for first ten oscillation modes in our model example are pictured on the Fig. 5.9. Further, if we want to compute successive (or other) part of the spectra, we can use shift and come back to the solving of eigenvalue problem. If we find several oscillation modes with high values of electromechanical coupling coefficient, we can use them as shifts and recompute the whole process for finer mesh.

[6] It equals to the process described in Paragraph 4.2.1

[7] Frequencies corresponding to the same modes, computed with different shifts, were considerably different.

### 5.4.2 Visualization of results

Selected oscillation modes can be visualized in GMSH software. Using the computed Ritz vectors from *results.dta* file, we write out the $*.pos$ file, which is the collection of nodes coordinates and values of displacement in each individual direction. Such file and its visualization, compiled for the third computed mode of our example, are shown on Fig. 5.10.

GMSH software allows to open $*.geo$ file (geometry) and $*.msh$ file (mesh) along with the $*.pos$ file. All introduced figures include the geometry. GMSH software allows to see the results spatially and manipulate with the visualized objects. It also provides the creation of animations.

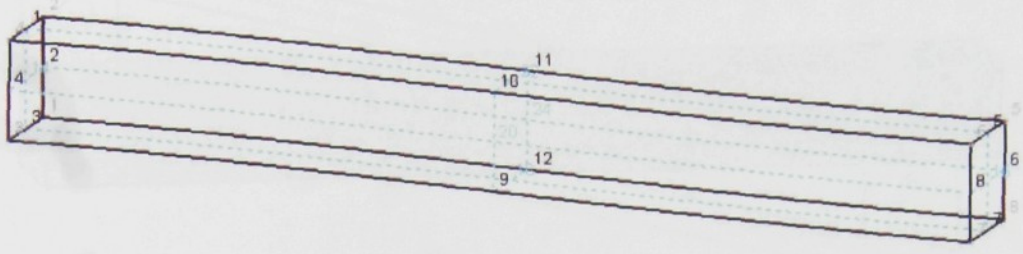


```
h = 0.35;
Point(1) = {0,0,0,h};
Point(2) = {0,1,0,h};
Point(3) = {0,0,1,h};
Point(4) = {0,1,1,h};
Point(5) = {10,1,0,h};
Point(6) = {10,1,1,h};
Point(7) = {10,0,1,h};
Point(8) = {10,0,0,h};
Line(1) = {4,2};
Line(2) = {2,1};
Line(3) = {1,3};
Line(4) = {3,4};
Line(5) = {6,5};
Line(6) = {5,8};
Line(7) = {8,7};
Line(8) = {7,6};
Line(9) = {3,7};
Line(10) = {4,6};
Line(11) = {2,5};
Line(12) = {1,8};
Line Loop(13) = {4,1,2,3};
Plane Surface(14) = {13};
Line Loop(15) = {8,5,6,7};
Plane Surface(16) = {15};
Line Loop(17) = {-9,-3,12,7};
Plane Surface(18) = {17};
Line Loop(19) = {-8,-9,4,10};
Plane Surface(20) = {19};
Line Loop(21) = {-11,-1,10,5};
Plane Surface(22) = {21};
Line Loop(23) = {-12,-2,11,6};
Plane Surface(24) = {23};
Surface Loop(25) = {20,16,22,24,18,14};
Volume(26) = {25};
```

discretization parameter

definition of points

definition of lines

definition of surfaces

definition of whole volume

Figure 5.3: Geometry and *.geo file of the piezoelectric beam.

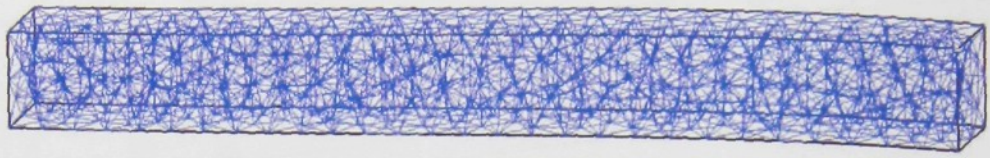

```
$NOD
559                 number of nodes
1 0 0 0             node number (the numbering may not start from 1) and its x, y, z coordinates
2 0 1 0
3 0 0 1
.
.
.
612 6.652253355392612 0.5051134969503318 0.77296910429609
613 1.982461835165782 0.2247649463461817 0.451403733503034
614 1.256197302270417 0.5004742451630535 0.7956230899769142
$ENDNOD
$ELM
2971                number of all elements (1D, 2D, 3D)
1 1 1 1 2 4 9
2 1 1 1 2 9 2       element number; type of the element - 1 = line, 2 = triangle, 3 = tetrahedron;
3 1 2 2 2 2 10      number of the physical entity to which the element belongs;
.                   number of the elementary entity to which the element belongs;
.                   number of nodes of this element; list of node numbers for this element
.
128 1 12 12 2 124 8
129 2 14 14 3 10 1 126
130 2 14 14 3 12 4 127
131 2 14 14 3 2 10 128
.
.
.
916 2 24 24 3 5 14 377
917 4 26 26 4 15 545 130 133
918 4 26 26 4 9 567 125 128
919 4 26 26 4 44 493 45 244
.
.
.
2970 4 26 26 4 161 509 166 458
2971 4 26 26 4 528 199 218 518
$ENDELM
```

nodes

1D elements

2D elements

3D elements

Figure 5.4: Example of the mesh and corresponding *.msh file.

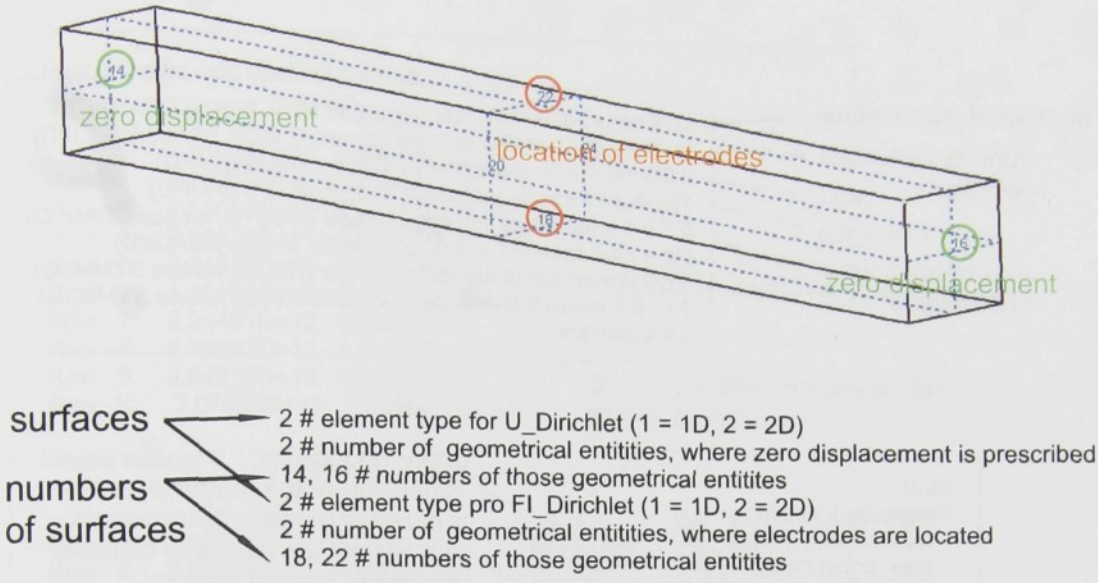


Figure 5.5: Example of the boundary conditions and corresponding text file.

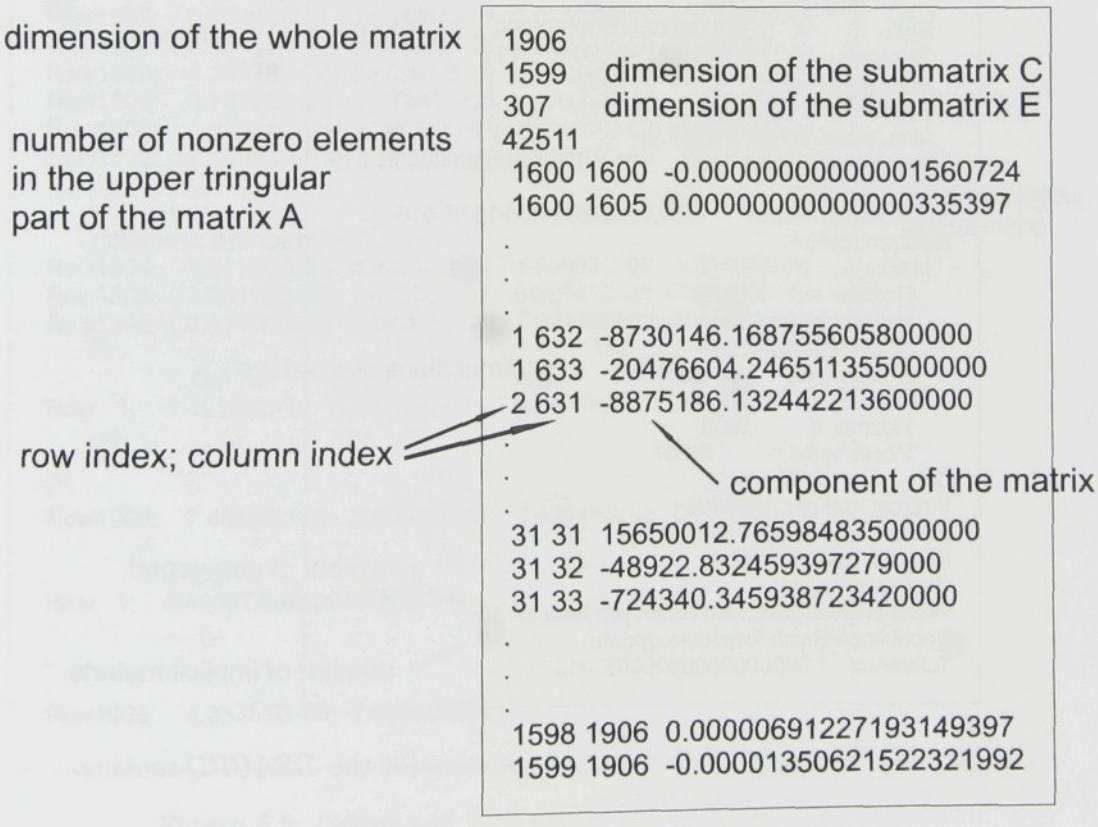


Figure 5.6: Example of the matrix $\mathbb{A}$ stored in SSC format.

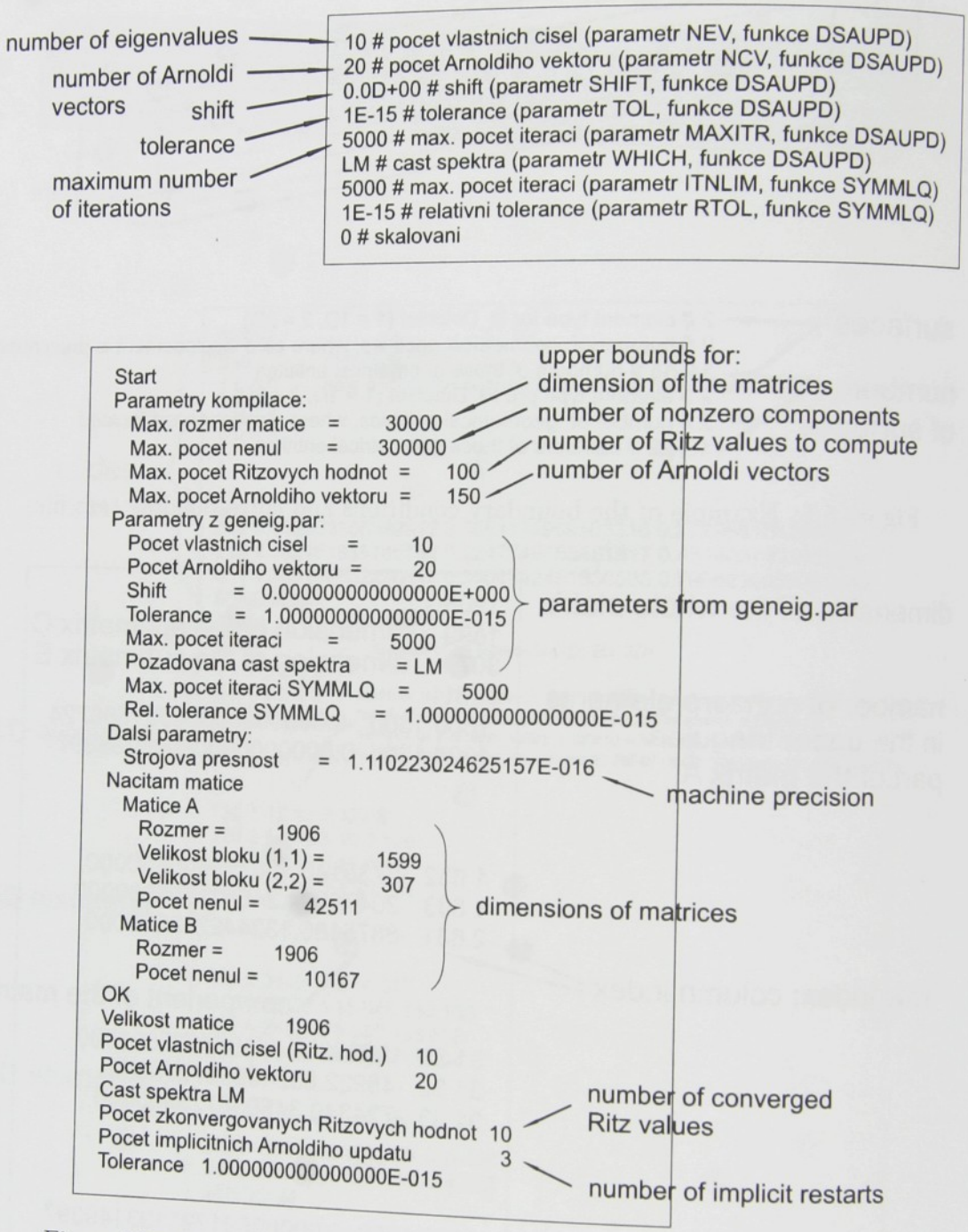


Figure 5.7: Example of the input parameters for the *DSAUPD* routine.

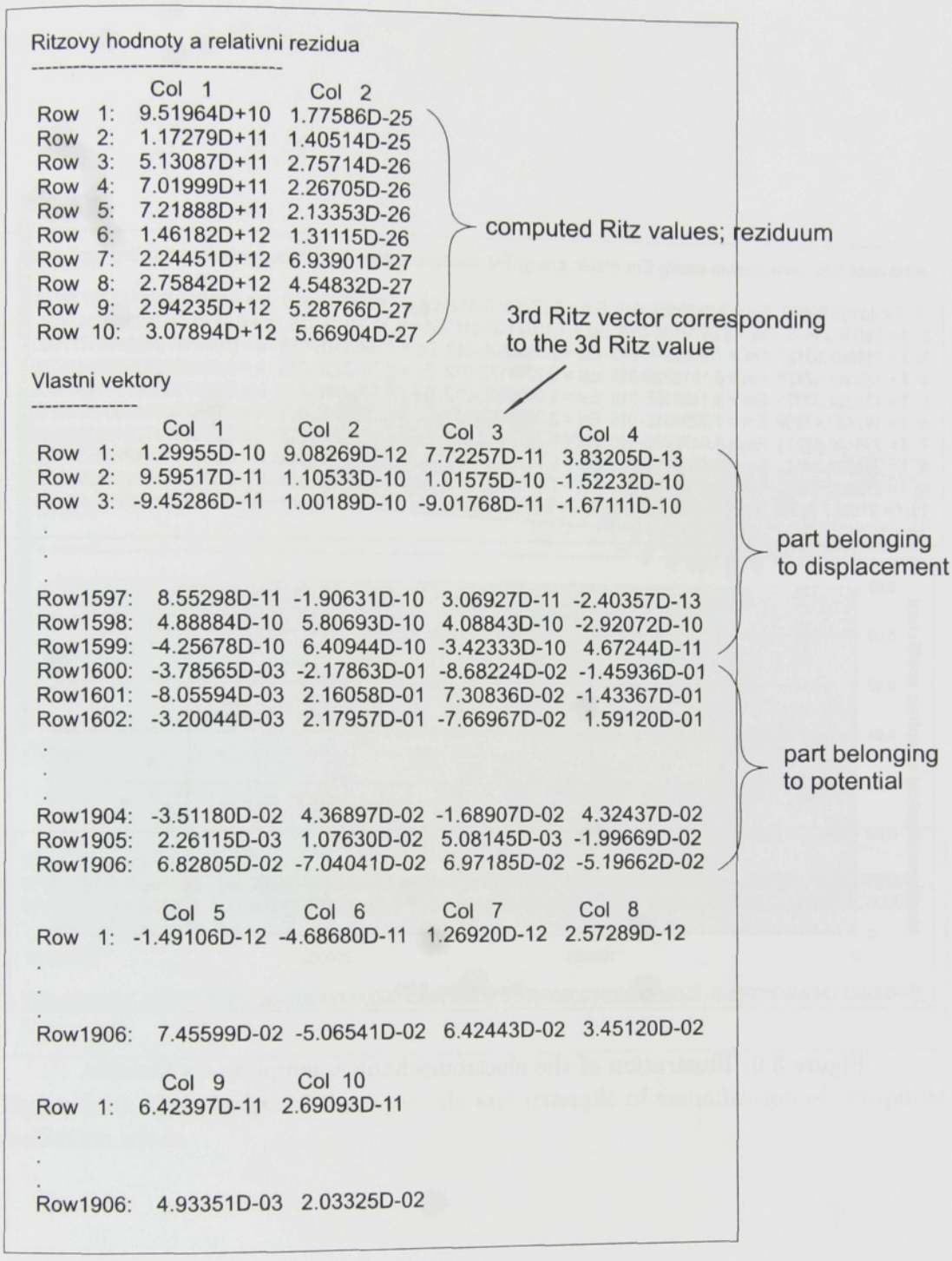


Figure 5.8: Computed Ritz values (above) and Ritz vectors.

resonance frequency, mutual energy Em, elastic energy Est, dielectric energy Ed, electromechanical coupling coefficient k

1: f = 49105.52903 Em = 7.683855E-015 Est = 3.770966E-012 Ed = 7.683850E-015 k = 0.04514019848229772200
2: f = 54504.23629 Em = 8.097010E-015 Est = 1.109414E-011 Ed = 8.097021E-015 k = 0.02701563828431043400
3: f = 114002.83127 Em = 7.306534E-015 Est = 2.585680E-012 Ed = 7.306537E-015 k = 0.05315794628831177500
4: f = 133348.57479 Em = 6.161322E-015 Est = 5.221013E-012 Ed = 6.161323E-015 k = 0.03435259269592815700
5: f = 135224.39371 Em = 8.145016E-015 Est = 8.090586E-012 Ed = 8.145016E-015 k = 0.03172896975416886900
6: f = 192427.47509 Em = 7.229451E-015 Est = 2.209906E-012 Ed = 7.229454E-015 k = 0.05719600189045234700
7: f = 238440.98321 Em = 8.047827E-015 Est = 6.391846E-012 Ed = 8.047829E-015 k = 0.03548347261693336100
8: f = 264332.35679 Em = 6.496615E-015 Est = 5.702803E-012 Ed = 6.496613E-015 k = 0.03375199429819311000
9: f = 273002.92338 Em = 4.859743E-015 Est = 7.170305E-012 Ed = 4.859746E-015 k = 0.02603380818148812500
10: f = 279267.72332 Em = 7.358814E-015 Est = 2.076271E-012 Ed = 7.358810E-015 k = 0.05953358695308058 60

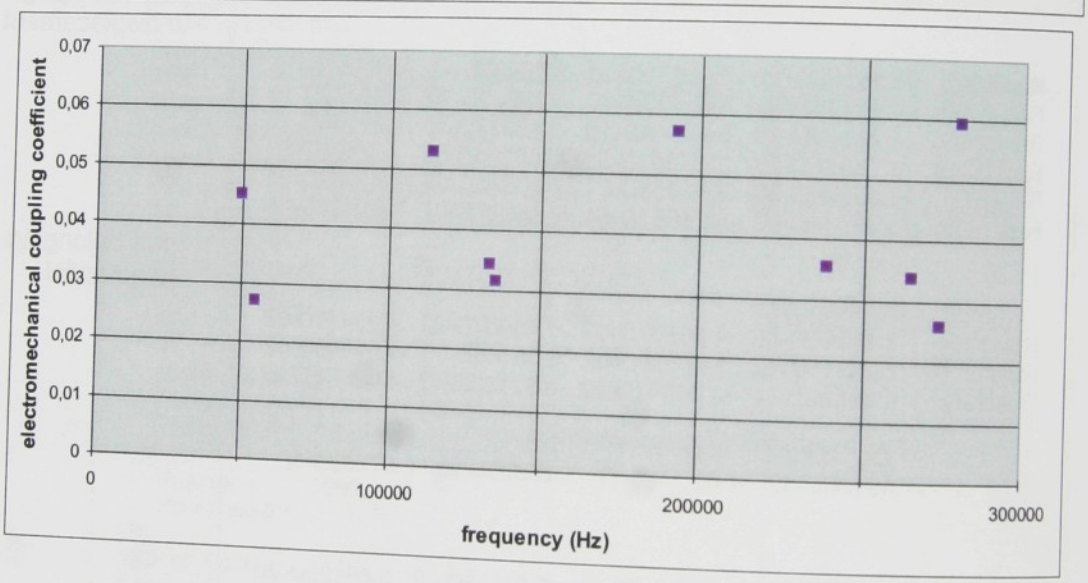


Figure 5.9: Illustration of the electromechanical coupling coefficients.

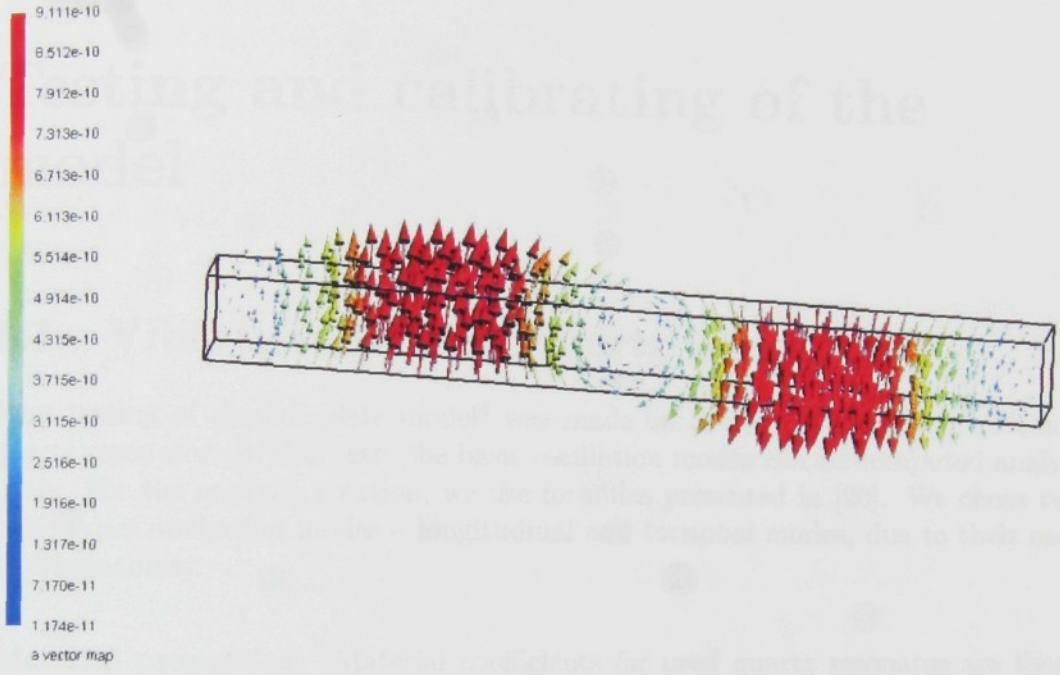


Figure 5.10: Illustration of the $*.pos$ file and example of visualization of computed oscillation mode.

# Chapter 6

# Testing and calibrating of the model

## 6.1 Vibration of beam quartz resonator

First testing of the complete model[8] was made on the oscillation modes of beam quartz resonator. In this case, the basic oscillation modes can be computed analytically. For the analytic solution, we use formulas presented in [26]. We chose two basic types oscillation modes – longitudinal and torsional modes, due to their easy discriminability.

**Material properties.** Material coefficients for used quartz resonator are listed below.

$$\mathbb{C} = 10^9 \begin{bmatrix} 86.740000 & 0.059173 & 18.840827 & 15.447720 & 0.000000 & 0.000000 \\ 0.059173 & 113.573454 & 14.543072 & -9.437720 & 0.000000 & 0.000000 \\ 18.840827 & 14.543072 & 75.100402 & 1.996143 & 0.000000 & 0.000000 \\ 15.447720 & -9.437720 & 1.996143 & 60.573072 & 0.000000 & 0.000000 \\ 0.000000 & 0.000000 & 0.000000 & 0.000000 & 53.203411 & 19.592742 \\ 0.000000 & 0.000000 & 0.000000 & 0.000000 & 19.592742 & 44.616585 \end{bmatrix},$$

$$\mathbb{D} = \begin{bmatrix} 0.002307 & -0.000043 & -0.002210 & 0.000941 & 0.000000 & 0.000000 \\ 0.000000 & 0.000000 & 0.000000 & 0.000000 & 0.001458 & -0.000875 \\ 0.000000 & 0.000000 & 0.000000 & 0.000000 & -0.003774 & 0.002159 \end{bmatrix},$$

$$\mathcal{E} = 10^{-11} \begin{bmatrix} 39.210000 & 0.000000 & 0.000000 \\ 0.000000 & 40.826035 & 0.574121 \\ 0.000000 & 0.574121 & 39.413965 \end{bmatrix}.$$

[8] The testing of particular physical parts of the model (separate elastic part or separate electric part) was made e.g. in [37].

Matrix of elastic coefficients $\mathbb{S} = \mathbb{C}^{-1}$ is equal to

$$\mathbb{S} = 10^{-11} \begin{bmatrix} 1.276986 & 0.013604 & -0.314674 & -0.313175 & 0 & 0 \\ 0.0136044 & 0.916211 & -0.184699 & 0.145369 & 0 & 0 \\ -0.314674 & -0.184699 & 1.446160 & 0.003815 & 0 & 0 \\ -0.313175 & 0.145369 & 0.003815 & 1.753290 & 0 & 00 \\ & 0 & 0 & 0 & 2.242175 & -0.984619 \\ 0 & 0 & 0 & 0 & -0.984619 & 2.673700 \end{bmatrix}.$$

Let us suppose these dimensions of the resonator:

$$l = 0.01 \text{ m}, \quad a, b = 0.001 \text{ m}.$$

The beam was fixed at both sides (see Fig. 6.2). The geometry and the mesh are shown on Fig. 5.3 and Fig. 5.4[9].

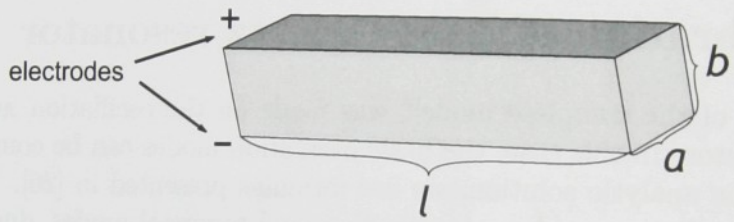


Figure 6.1: Piezoelectric beam with electrodes exciting odd longitudinal oscillation.

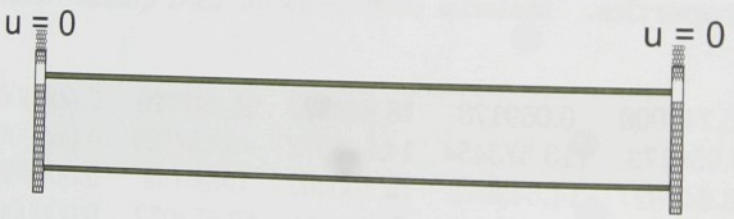


Figure 6.2: Prescribed boundary conditions.

### 6.1.1 Longitudinal oscillation modes

First comparison was made by computing of longitudinal vibrational modes. These modes can be excited by the electrodes placement shown on the Fig. 6.1. For $h$-th eigenfrequency holds the basic relation [26]

$$f_h = \frac{h}{2l}\sqrt{\frac{1}{\varrho s_{11}}}, \quad h = 1, 2, 3, \ldots \tag{6.1}$$

[9]This is only exemplary picture of coarser discretization than the one that was really used.

The number $s_{11}$ is the first elastic coefficient and is equal to $\mathbb{S}_{11}$. The equation is efficient enough for beams, whose longitudinal dimension is large compared to the cross-section. If we take into account the correction to the profile of the beam (dimensions $a$ and $b$), we obtain better results using the more complicated relation

$$f_h = \frac{hf_1}{\sqrt{1 + \frac{\pi^2 h^2 \mu^2 (a^2+b^2)}{12l^2}}},$$

where the Poisson ratio $\mu$ can be computed from

$$\frac{1}{s_{44}} = \frac{1}{2s_{11}(1+\mu)}.$$

So the spectrum of the harmonic oscillation is thickening for increasing $h$, while the basic relation (6.1) supposes the higher resonance frequencies as integer multiples of the first frequency.

One side of the resonator was fixed. For the parameters mentioned above, the frequencies of the longitudinal vibrations (computed analytically) are

$$\begin{aligned} f_1 &= 271803 \text{ Hz} \\ f_2 &= 543606 \text{ Hz} \\ f_3 &= 815409 \text{ Hz} \\ f_4 &= 1087212 \text{ Hz} \\ f_5 &= 1359015 \text{ Hz} \\ f_6 &= 1630818 \text{ Hz} \\ &\vdots \end{aligned}$$

**Computed frequencies** First six computed modes are shown on the Fig. 6.3, 6.4 and 6.5. Appropriate frequencies are listed below.

| | frequency | relative difference (%) |
|---|---|---|
| $f_1 =$ | 286205 Hz | +5.3 |
| $f_2 =$ | 572561 Hz | +5.3 |
| $f_3 =$ | 859212 Hz | +5.4 |
| $f_4 =$ | 1146292 Hz | +5.4 |
| $f_5 =$ | 1433952 Hz | +5.5 |
| $f_6 =$ | 1722252 Hz | +5.6 |
| $\vdots$ | | |

Parameters of the computation were[10]:

Mesh: number of nodes = 4258, number of elements = 21326
Matrices: matrix $\mathbb{A}$ $7476 \times 7476$, 102446 nonzero elements in upper tringular part, matrix $\mathbb{B}$ 21326 nonzero elements in upper tringular part

[10]The spatial reduction to the $x$-direction was used.

### 6.1.2 Torsional oscillation

Second problem was computing of torsional modes, where the proper boundary condition was also used from [26]. For $h$-th eigenfrequency holds the basic relation

$$f_h = \frac{h}{2l}\sqrt{\frac{G}{\varrho}}\frac{2\frac{a}{b}}{\sqrt{1+(\frac{a}{b})^2}}\sqrt{1-\frac{a}{b}\chi\left(\frac{a}{b}\right)}, \quad h = 1, 2, 3, ... \tag{6.2}$$

The effective torsional modulus $G$ can be approximated according to

$$\sqrt{G} = \frac{\frac{b^2}{\sqrt{s_{66}}} + \frac{a^2}{\sqrt{s_{55}}}}{a^2 + b^2}$$

and for our case is $G = 40973043485.312064$. The term $\chi(\frac{a}{b})$ can be expressed as

$$\chi\left(\frac{a}{b}\right) \doteq \left(\frac{4}{\pi}\right)^5 \frac{3}{16}\left(\tanh\frac{\pi b}{2a} + 0.00452\right)$$

and for our case is equal to $\chi\left(\frac{a}{b}\right) = 0.5777787$.

Analytically computed frequencies are

$$\begin{aligned}
f_1 &= 180668 \text{ Hz} \\
f_2 &= 361336 \text{ Hz} \\
f_3 &= 542004 \text{ Hz} \\
f_4 &= 722672 \text{ Hz} \\
f_5 &= 903340 \text{ Hz} \\
f_6 &= 1084008 \text{ Hz} \\
f_7 &= 1264676 \text{ Hz} \\
f_8 &= 1445344 \text{ Hz} \\
f_9 &= 1626012 \text{ Hz} \\
&\vdots
\end{aligned}$$

**Computed frequencies** First eight computed modes are shown on the Fig. 6.6 - Fig. 6.9. Appropriate frequencies are listed below.

| | frequency | relative difference (%) |
|---|---|---|
| $f_1 =$ | 171615 Hz | −5 |
| $f_2 =$ | 356761 Hz | −1.3 |
| $f_3 =$ | 532879 Hz | −1.7 |
| $f_4 =$ | 707107 Hz | −2.2 |
| $f_5 =$ | 853750 Hz | −5.5 |
| $f_6 =$ | 1024242 Hz | −5.5 |
| $f_7 =$ | 1189933 Hz | −6 |
| $f_8 =$ | 1361634 Hz | −5.8 |
| $f_9 =$ | 1627816 Hz | +0.1 |
| $\vdots$ | | |

Parameters of the computation were[11]:

Mesh: number of nodes = 4258, number of elements = 223087
Matrices: matrix $\mathbb{A}$ $8606 \times 8606$, 223087 nonzero elements in upper triangular part, matrix $\mathbb{B}$ 49026 nonzero elements in upper tringular part

**Comment - visualized results of testing examples.** Presented pictures are visualized in the GMSH software. The scale representative the absolute values of the displacement is here only illustrative, because the eigenvectors are normalized according to [9]

$$\mathrm{U}^T \mathbb{M} \mathrm{U} = \mathbb{I}.$$

[11] Full spatial problem was solved.


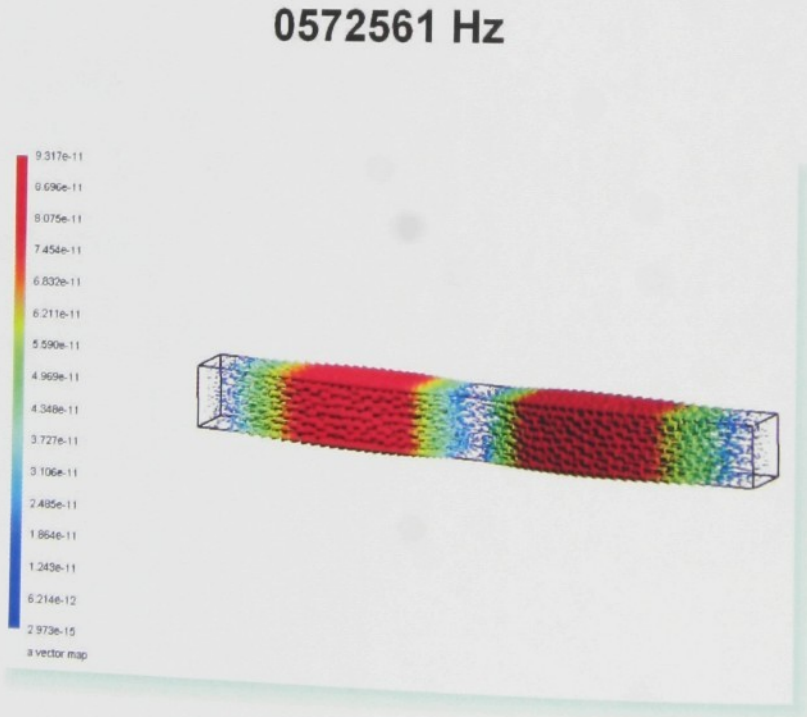


Figure 6.3: First two longitudinal oscillation modes of the piezoelectric beam.

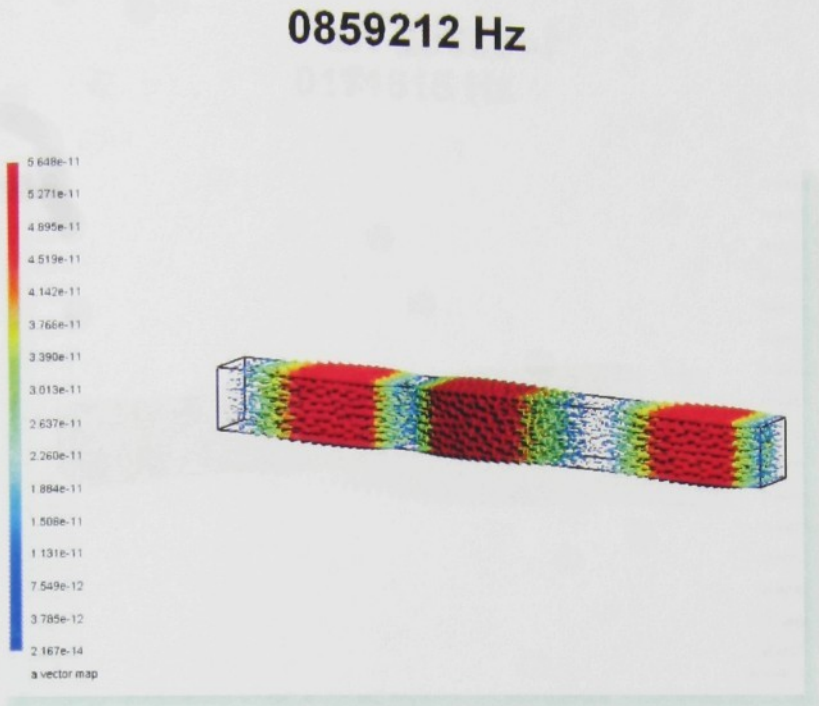


Figure 6.4: Second couple of longitudinal oscillation modes of the piezoelectric beam.


Figure 6.5: Fifth and sixth longitudinal oscillation modes of the piezoelectric beam.

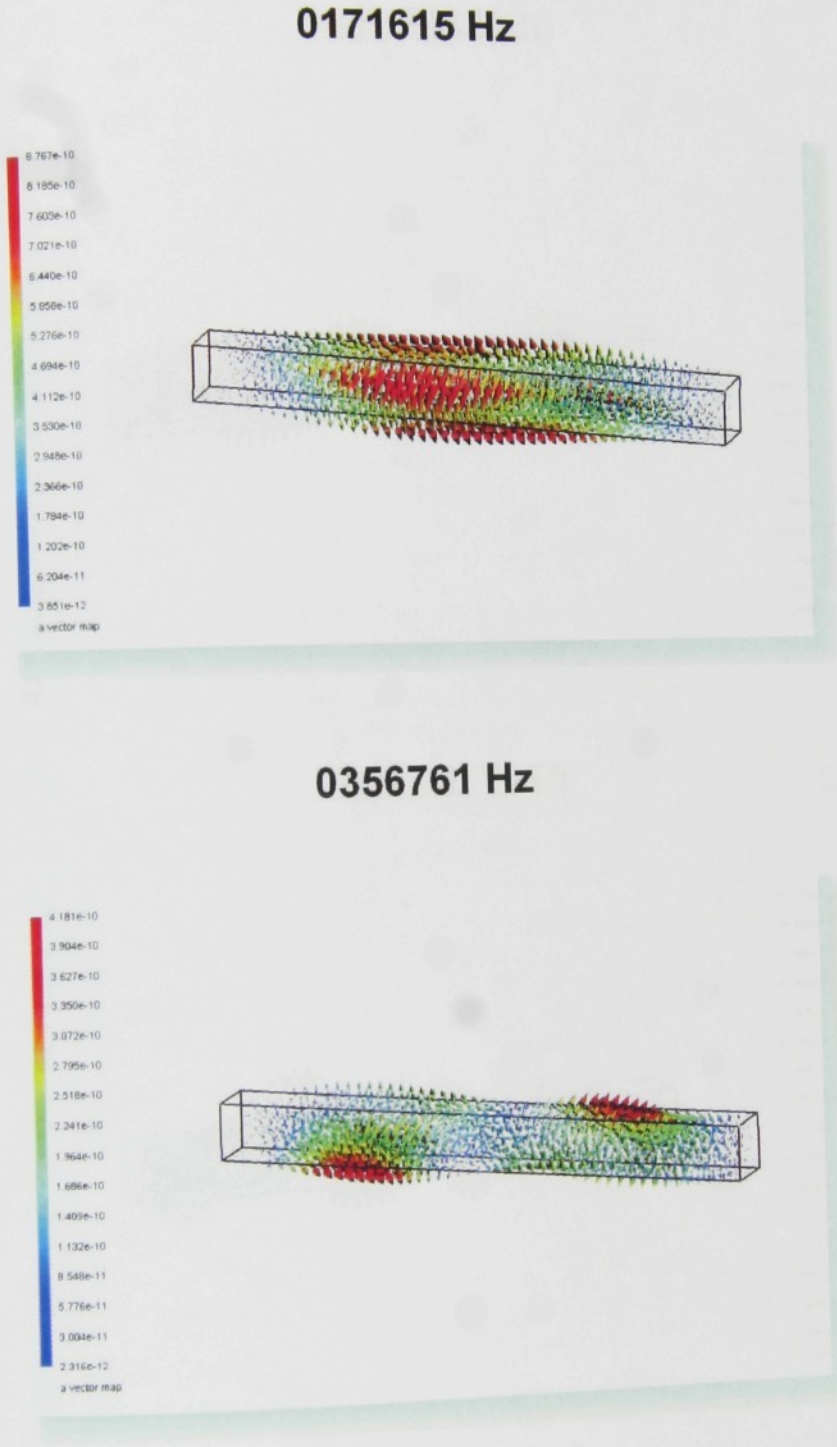


Figure 6.6: First two torsional oscillation modes of the piezoelectric beam.

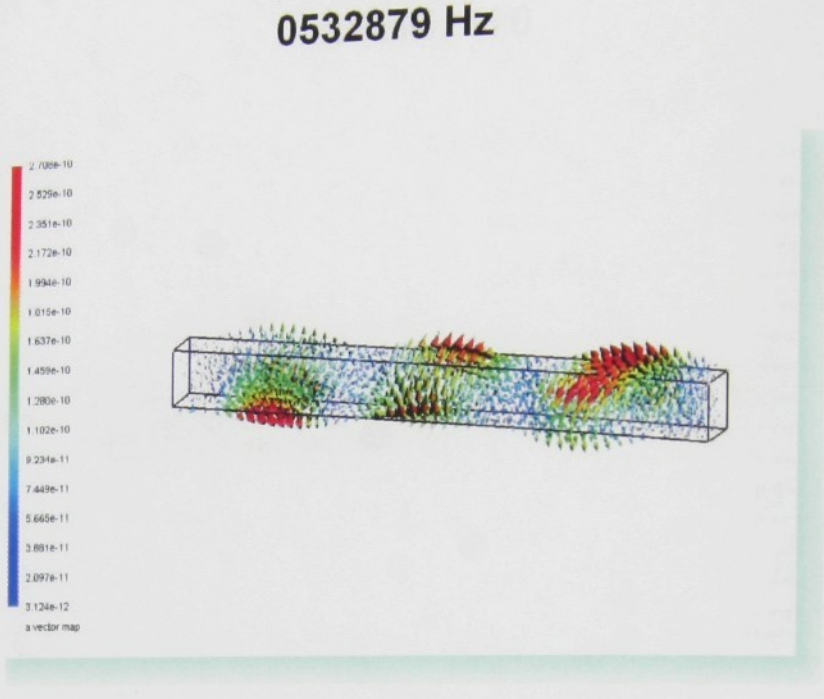


Figure 6.7: Second couple of torsional oscillation modes of the piezoelectric beam.

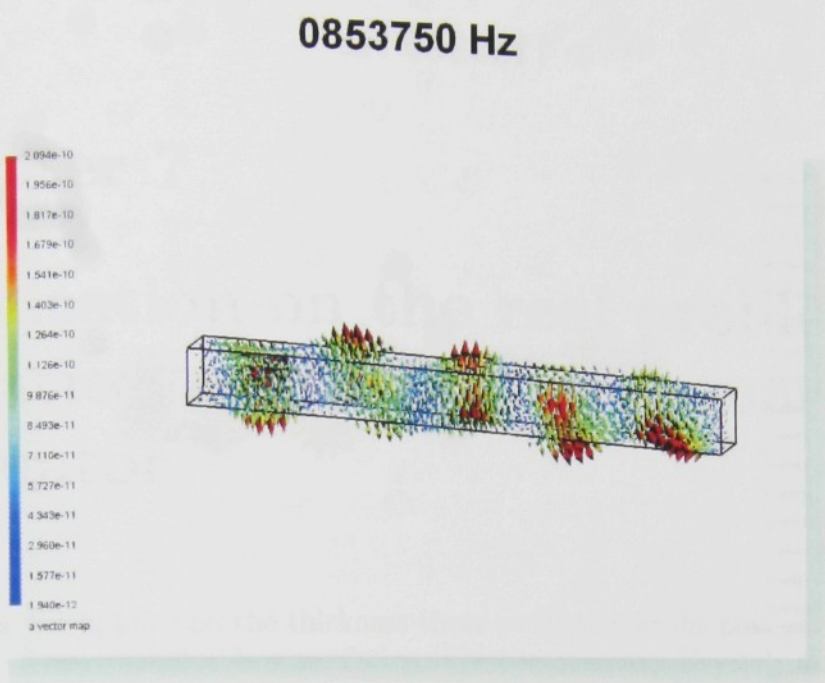


Figure 6.8: Third couple of torsional oscillation modes of the piezoelectric beam.

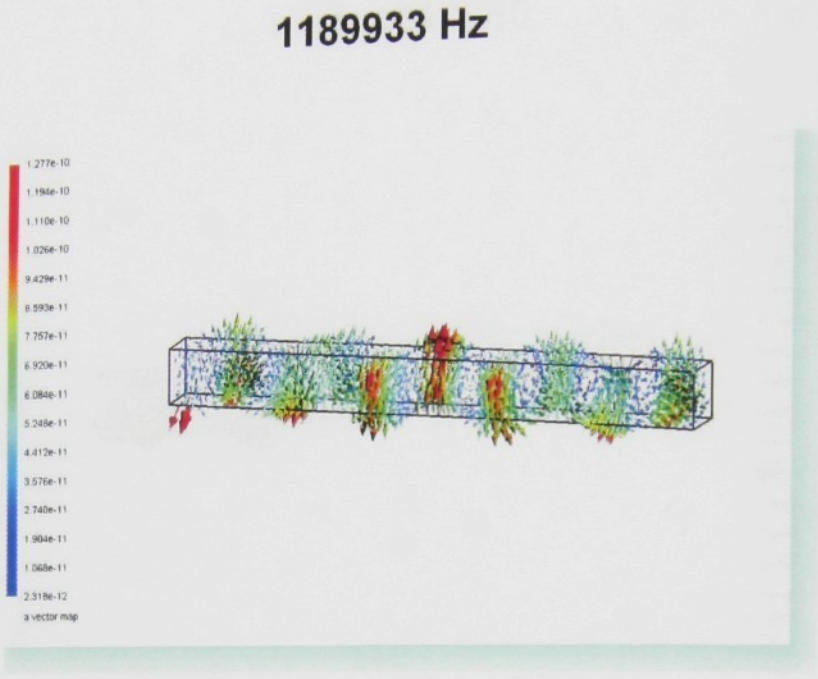


Figure 6.9: Seventh and eighth torsional oscillation modes of the piezoelectric beam.

# Chapter 7

# Application on the real problem - vibration of plan parallel quartz resonator

The model was applied on the thickness-shear oscillation of the plan parallel quartz resonator. This resonator is manufactured in the company Krystaly, a.s., resident in Hradec Králové [35]. We looked for dominant modes in $x$ direction.

The geometry and the illustrative mesh of the resonator are shown on the Fig. 7.1. It is a circular wafer with radius $R$ including two circular electrodes with radius $r$ placed in the middle of upper and bottom side. The resonator is fixed in two opposite spots in $x$ direction. The thickness of the resonator is $h$. All parameters are listed in the Tab. 7.1.

The resonator is made form quartz $AT - cut_{35.25°}$ The material constants are

$$\mathbb{C} = 10^9 \begin{bmatrix} 86.74 & -8.25 & 27.15 & -3.66 & 0.0 & 0.0 \\ -8.25 & 129.77 & -7.42 & 5.7 & 0.0 & 0.0 \\ 27.15 & -7.42 & 102.83 & 9.92 & 0.0 & 0.0 \\ -3.66 & 5.7 & 9.92 & 38.61 & 0.0 & 0.0 \\ 0.0 & 0.0 & 0.0 & 0.0 & 68.81 & 2.53 \\ 0.0 & 0.0 & 0.0 & 0.0 & 2.53 & 29.01 \end{bmatrix},$$

$$\mathbb{D} = \begin{bmatrix} 0.002307 & -0.000043 & -0.002210 & 0.000941 & 0.000000 & 0.000000 \\ 0.000000 & 0.000000 & 0.000000 & 0.000000 & 0.001458 & -0.000875 \\ 0.000000 & 0.000000 & 0.000000 & 0.000000 & -0.003774 & 0.002159 \end{bmatrix},$$

$$\mathcal{E} = 10^{-11} \begin{bmatrix} 39.210000 & 0.000000 & 0.000000 \\ 0.000000 & 40.826035 & 0.574121 \\ 0.000000 & 0.574121 & 39.413965 \end{bmatrix}.$$

| $R$ (mm) | $r$ (mm) | $h$ (mm) |
|---|---|---|
| 7 | 4.5 | 0.333 |

Table 7.1: Proportions of resonator sample.

| Resonance frequency | Measured (kHz) | Computed (kHz) | Relative difference |
|---|---|---|---|
| basic | 4962 | 4210.843 | 15.1% |
| 1. harmonic | $5067.5 = 1.02\ f_1$ | $4246.481 = 1.01\ f_1$ | 16.2% |
| 2. harmonic | $5102.5 = 1.03\ f_1$ | $4331.652 = 1.03\ f_1$ | 14.7% |

Table 7.2: Comparison of measured and computed dominant resonant frequencies of thickness-shear vibrational modes.

For listed results, parameters of the computation were[13]:

Mesh: number of nodes = 7360, number of elements =31860
Matrices:
matrix $\mathbb{A}$ $9771 \times 9771$, 100430 nonzero elements of upper tringular part,
matrix $\mathbb{B}$ 47038 nonzero elements of upper tringular part
Computational time:
preprocessing part $\sim 3\ min$, processing part (for 400 eigenvalues) $\sim 55\ min$,
postprocessing part $\sim 1\ min$

Memory demands (for 400 eigenvalues) $\sim 0.8$ GB
Computer equipment: PC, Celeron CPU 2.6 GHz, 1 GB RAM

Experimental measured results were obtained from the development department of Krystaly, a.s. The measurement output (shown on Fig. 7.2) describes the phase and shift phase dependance on the excitation frequency, with marked resonant frequencies.

## 7.1 Results

Table 7.2 shows the comparison between measured and computed three dominant resonant frequencies of thickness-shear vibration. The average deviation of computed results form the measurement is rather high, about 15%, but the relative distances between particular frequencies are well-kept.

Graph of electromechanical coupling coefficients, from which the dominant frequencies can be located easily, is shown on the Fig. 7.3.

On the next several pages, the visualized experimental results are compared to the ideal theoretical state. Each time, first page shows the ideal state: active vibrational

[13]The spatial reduction to the $x$-direction was used.

sections, amplitudes distribution on axis $y$ at the upper plate of the resonator and vertical cut. Aside from this, the second page shows the measured results: whole resonator with displayed amplitudes, schematic amplitudes distribution on axis $y$ at the upper plate of the resonator and vertical cut.

The presented results were obtained from the computation with the parameters mentioned above. For finer meshes (leading to larger dimension of the eigenvalue problem), the computational time considerably increases, which is caused by the limited memory capacity. This fact can be partially avoided e.g. by several repetition of computations for a smaller number of eigenvalues.

The computed modes contain certain amount of the computational noise (mostly evident in the third dominant mode), but their types can be uniquely identified with the ideal states.

**Possible use of the results in the design process.** The model allows to follow up the resonators behavior depending on the changes in its shape properties. As an example, the graph on the Fig. 7.13 shows the dependance of the resonant frequencies on the change of the resonator thickness and the separation of the particular frequencies. The dependance of the resonant frequencies on the thickness should be linear. This fact is well represented by the model.

Such results can be used in the design process of the resonator, e.g. in the optimization process, when we look for such shape of the resonator, that would have the large distances between particular dominant resonant frequencies.

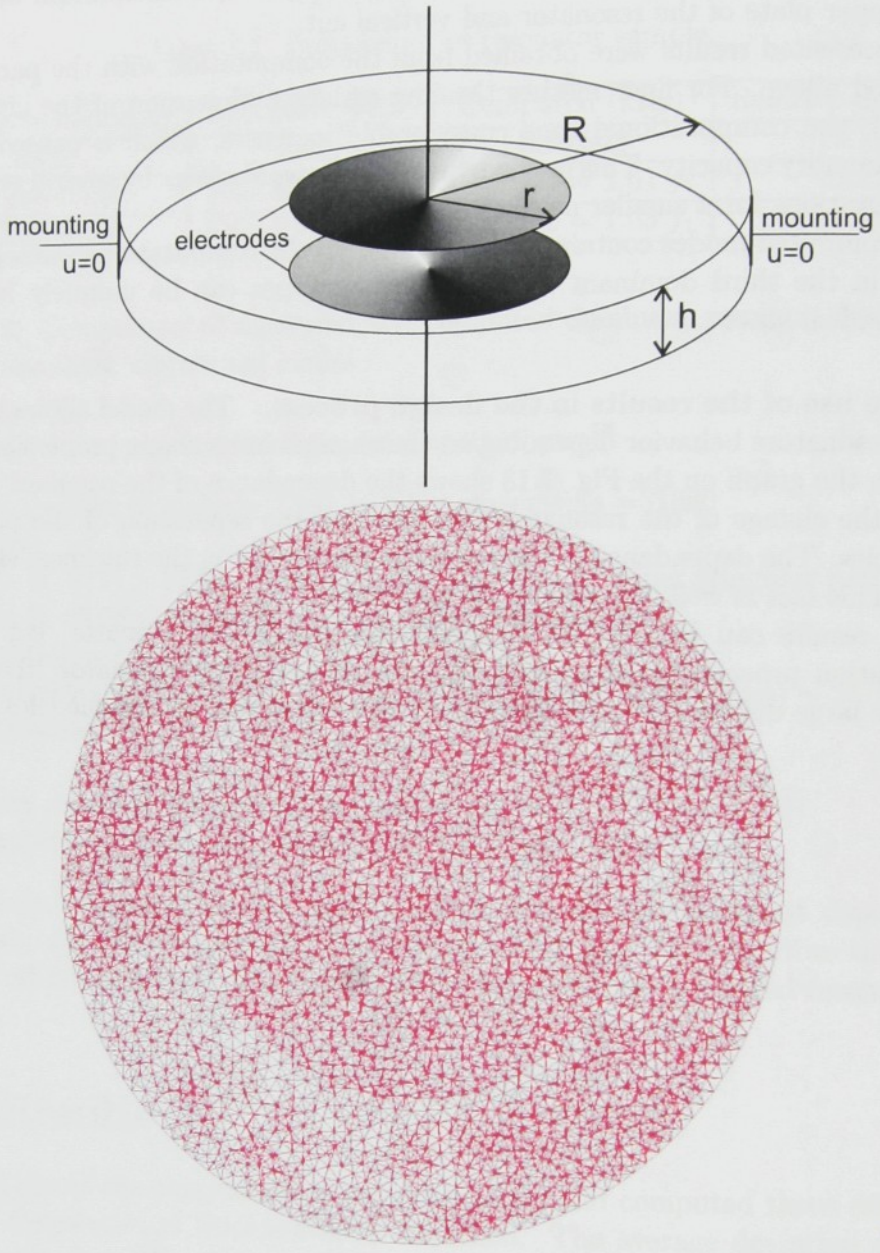


Figure 7.1: Geometry and illustrative mesh of plan parallel resonator.

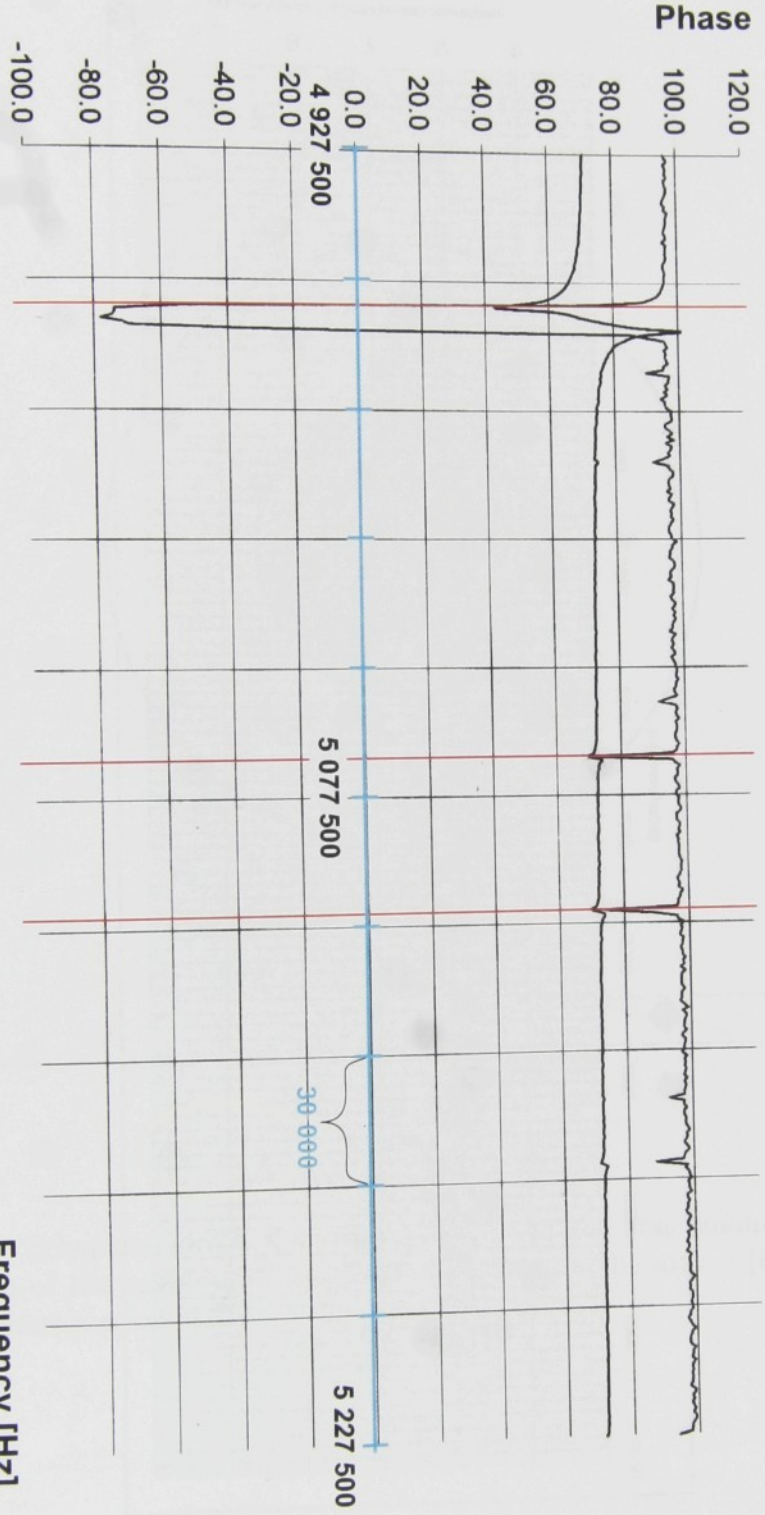


Figure 7.2: Phase dependance (upper line) and shift phase dependance (bottom line) on the excitation frequency. The maximal phases correspond to the resonances.

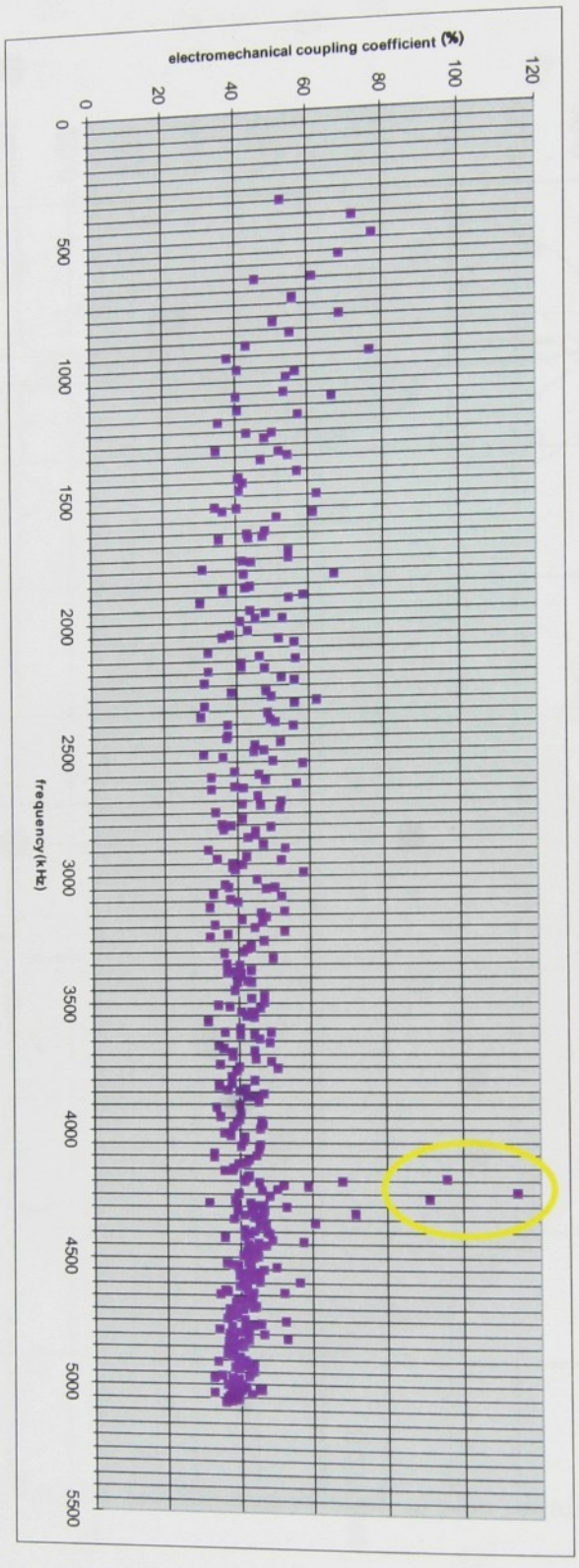


Figure 7.3: Graph of electromechanical coupling coefficients for first 400 resonant frequencies with marked three dominant oscillation modes.

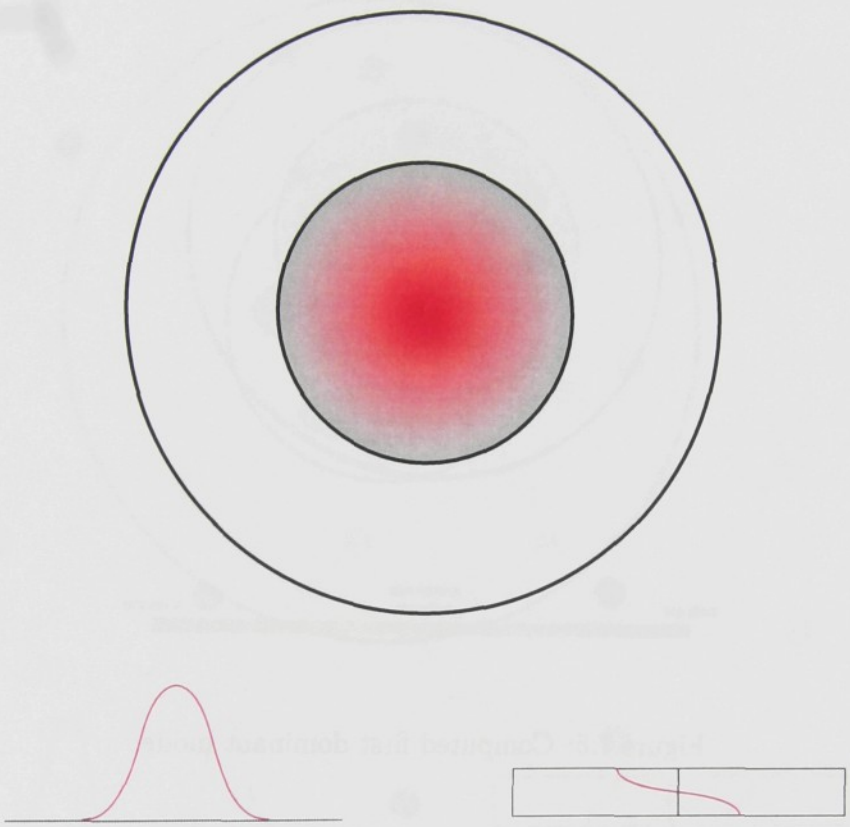

Figure 7.4: Schematic draft of theoretical shape of the first dominant mode and distribution of the amplitudes (in the $x$-direction) on the axis $y$ (left curve) and in the $yz$-plane median cut.

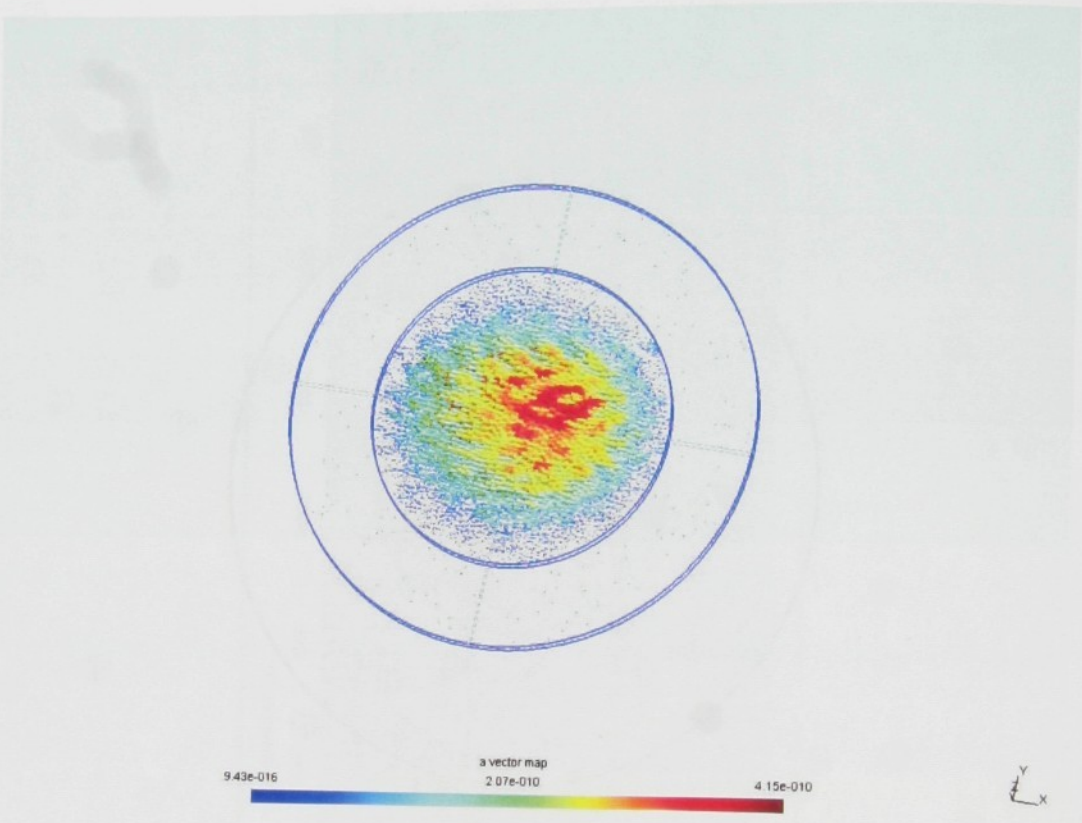


Figure 7.5: Computed first dominant mode.

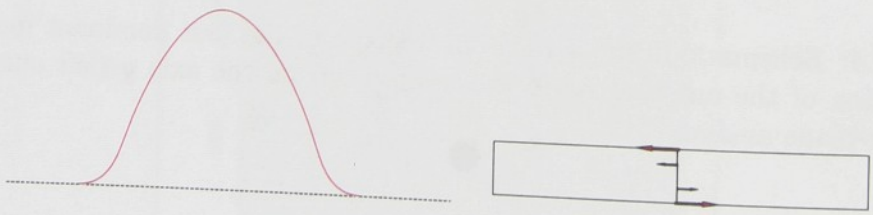

Figure 7.6: Curve of the amplitudes (in the $x$-direction) on the axis $y$ (left curve) and in the $yz$-plane median cut.

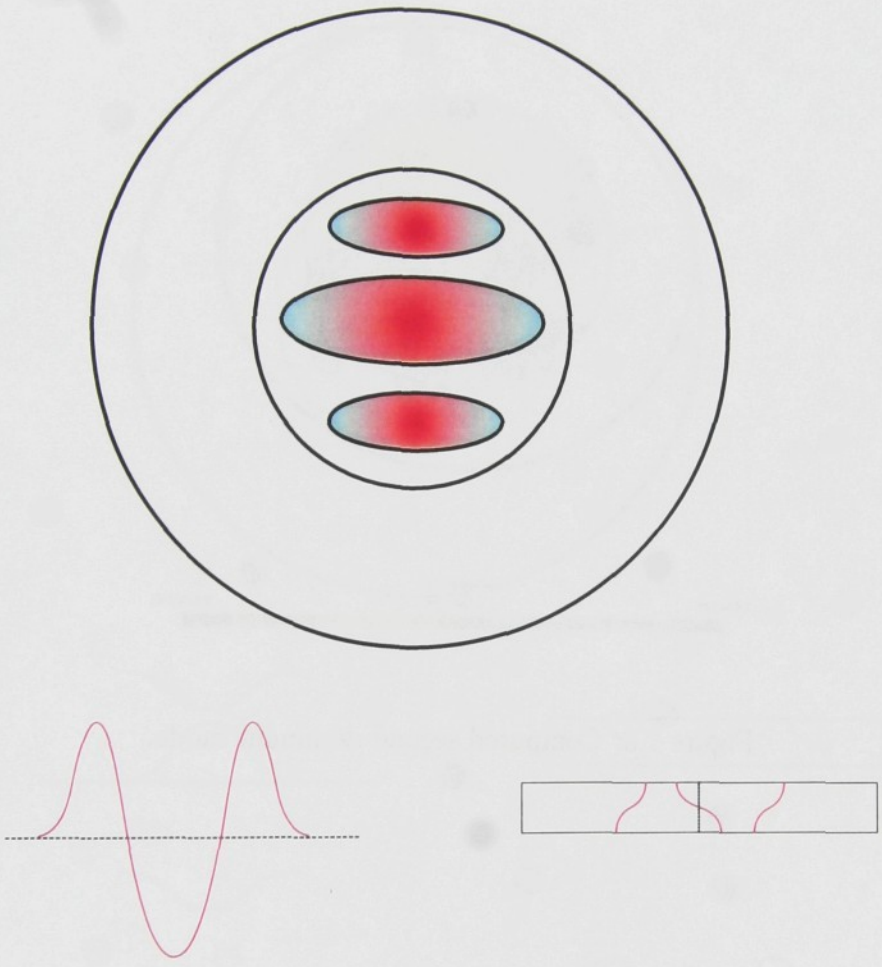

Figure 7.7: Schematic draft of theoretical shape of the second dominant mode and curve of the amplitudes (in the $x$-direction) on the axis $y$ (left curve) and in the $yz$-plane median cut.

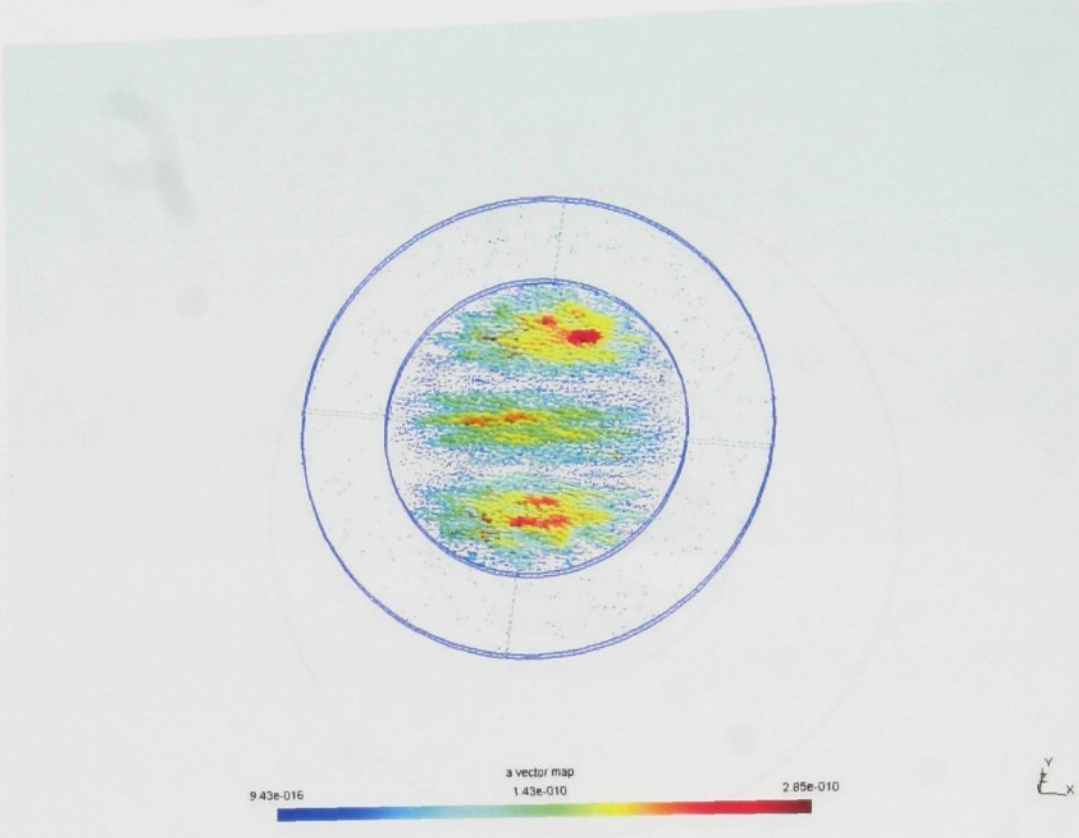


Figure 7.8: Computed second dominant mode.

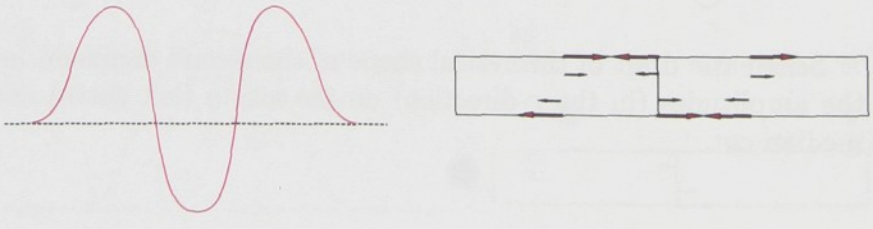

Figure 7.9: Curve of the amplitudes (in the $x$-direction) on the axis $y$ (left curve) and in the $yz$-plane median cut.

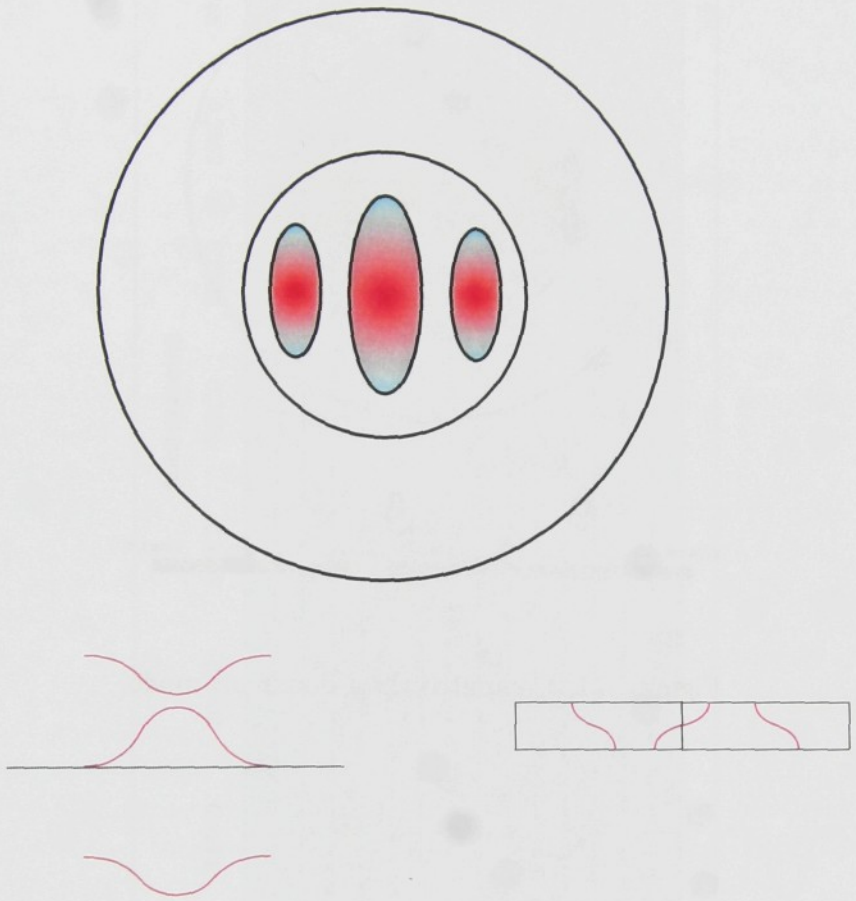

Figure 7.10: Schematic draft of theoretical shape of the third dominant mode and curve of the amplitudes (in the $x$-direction) on the axis $y$ (left curve) and in the $yz$-plane median cut.

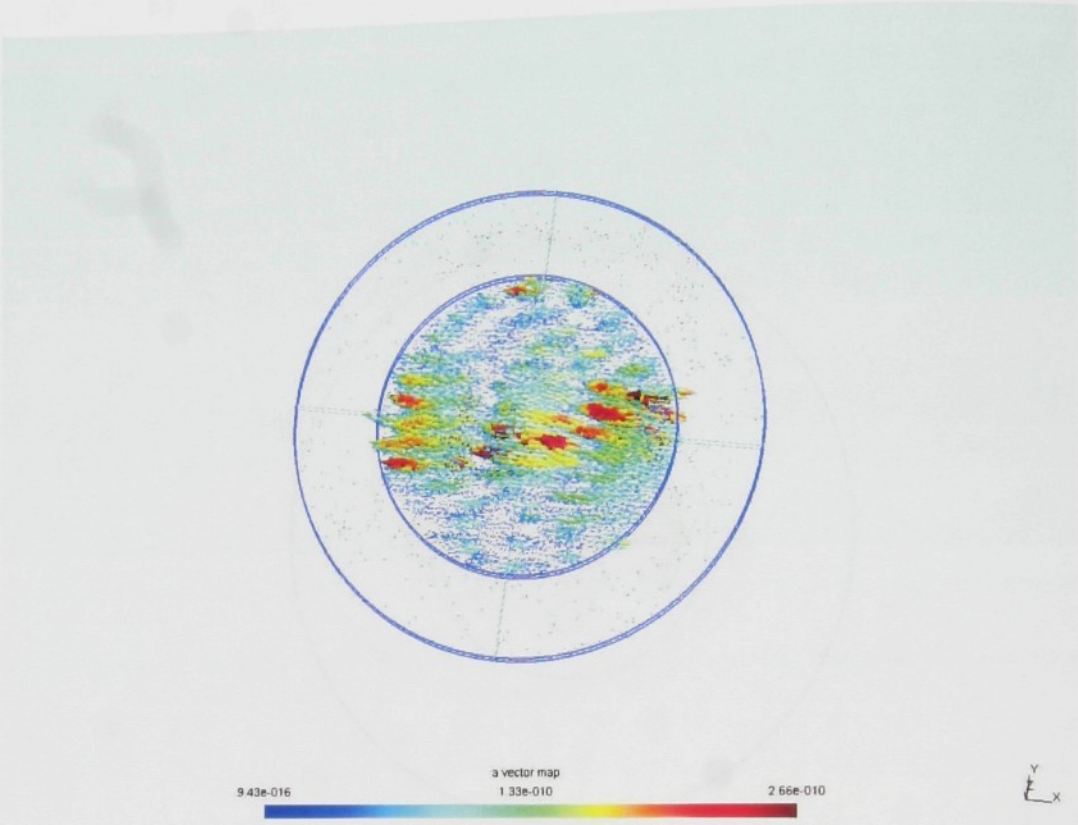


Figure 7.11: Computed third dominant mode.

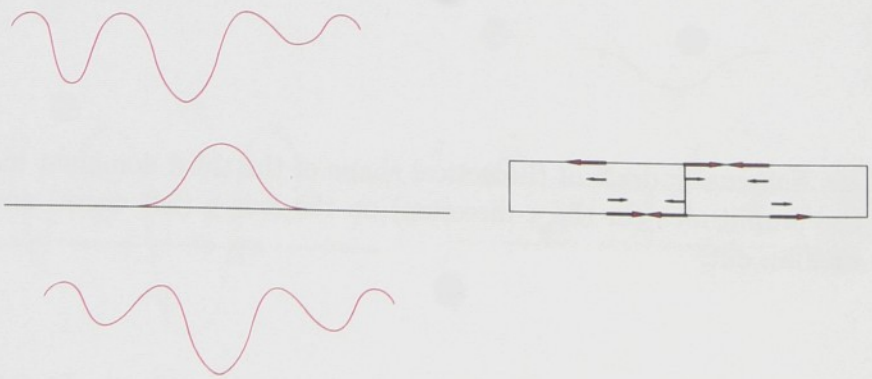

Figure 7.12: Curve of the amplitudes (in the $x$-direction) on the axis $y$ (left curve) and in the $yz$-plane median cut.

# Conclusion

The thesis presents the results in modelling of the resonant characteristic of piezoelectric resonators. Discretization of the physical model, based on the finite element method, leads to the generalized eigenvalue problem with large dimension, which is solved by using the iterative Krylov subspace methods, namely the implicitly restarted Arnoldi method.

The computer implementation of the model brings the comprehensive programme module, which is suitable for determination of the dominant resonant frequencies in real oscillation problems, including the various shaped resonators.

The testing problems confirm the applicability of the model, with computed results corresponding to the analytic solutions. The model, applied to the real task of the thickness–shear oscillation of the plan–parallel quartz resonator, brings qualitatively demonstrable agreement with the measurement and keeps the frequency separation in the right proportions. The shift between computed and measured dominant resonant frequencies shows the limitations of the model, but after the calibration to a reference instant, the implementation of the model can be used for practical computations. The model embodies accurate response to the change of the input parameters (e.g., it records the linear dependance of the resonant frequencies on the resonator's thickness).

There are some areas of interest for the future work. The main incoming task is to develop the optimization programme module, which would be suitable for the use in shape design process of new resonators. This involves to repeat the solution of the eigenvalue problems many times. With this objective, the need of a computer implementation running faster than the present–day one may arise – e.g. with the help of parallel computation.

As was mentioned in the paragraph 4.3.1, towards the quickness of computation stays the need of very fine meshes to express the complicated oscillation modes. This fact leads to algebraic problems with very large dimensions. The numerical algebraic methods, used in the model, have a good computational performance, but are limited by the memory size on the PC. The possible way to solve more extensive algebraic problems with keeping the good computational performance is using the implementation of multilevel eigenvalue methods (see, e.g., [2], [5] or [7]).

# Bibliography


[1] Allik H., Hughes T. J. R., *Finite element method for piezoelectric vibration*, International journal for numerical methods in engineering, Vol. 2, pp. 151-157, 1970.

[2] Bennighof J.K., Lehoucq R.B., *An automated multilevel substructuring method for eigenspace computation in linear elastodynamics*, SIAM, Vol. 25, 2003.

[3] Brenner S.C., Scott L.R., *The mathematical theory of finite element methods* Springer-Verlag NY, 1994.

[4] Brepta R., Pust L., Turek F., *Mechanické kmitání*, Technical Guide, Vol. 71, Sobotáles, Prague 1994.

[5] Chao Yang, *Solving large-scale eigenvalue problems in SciDAC applications*, Technical report, Lawrence Berkeley National Laboratory, 2005.

[6] Dulmet B., *Current trends of FEM applied to piezoelectric resonators*, ENSMM, L'institut FEMTO-ST, Besancon.

[7] Fialko S.Y., *An aggregation multilevel iterative solver with shift acceleration for eigenvalue analysis of large-scale structures*, CMM-2003 Computer Methods in Mechanics, Gliwice, 2003.

[8] Hwang W.S., Park H.Ch., *Closed form expression for higher-order electroelastic tetrahedral elements*, AIAA Journal, Vol. 31, No. 5, 1993.

[9] Lehoucq R., Maschhoff K., Sorensen D., Yang Ch.: *ARPACK USERS GUIDE, Solution of large scale eigenvalue problems by implicitly restarted Arnoldi methods*, 1997.

[10] Lerch R., *Simulation of piezoelectric devices by two- and three-dimensional finite elements*, IEEE Transactions on Ultrasonics, Ferroelectric and Frequency Control, Vol. 37, No. 2, 1990.

[11] Míka S., Kufner A., *Parciální diferenciální rovnice I*, SNTL Praha 1983.

[12] Milsom R. F., Elliot D. T., Terry Wood S., Redwood M., *Analysis and design of couple mode miniature bar resonator and monolothic filters,* IEEE Transactions on Ultrasonics, Ferroelectric and Frequency Control, Vol. 30, pp. 140- 155, 1983.

[13] Moetakef M. A., Lawrence K.L., Joshi S.P., Shiakolas S., *Closed form expression for higher-order electroelastic tetrahedral elements,* AIAA Journal, Vol. 33, No. 1, 1995.

[14] Nečas J., Hlaváček I., *Mathematical theory of elastic and elasto-plastic bodies: An introduction,* 1. ed., Elsevier, Amsterdam 1981.

[15] Piefort V., *Finite element modelling of piezoelectric active structures,* Ph.D. thesis, FAS ULB, 2001.

[16] Rektorys K., *Variační metody,* Academia Praha 1989.

[17] Samanta B., Ray M.C., Bhattacharyya R., *Finite element model for active control of intelligent structures,* AIAA Journal, Vol. 34, No. 9, 1996.

[18] Semenčenko V.K., *Izbrannye glavy teoretičeskoj fiziki,* Voennogo izdatelstvo Ministerstva oborony SSSR, Leningrad 1960.

[19] Sorensen D., *Implicitly restarted Arnoldi/Lanczos methods for large scale eigenvalue calculations, 1995.*

[20] Stewart G. W., *Matrix algorithms,* University of Maryland, College Park 1999.

[21] Štoll I., Tolar J., *Teoretická fyzika,* Czech Technical University, Prague 1981.

[22] Tiersten H.F., *Linear piezoelectric plate vibrations: Elements of the linear theory of piezoelectricity and the vibrations of piezoelectric plates,* Plenum Press, New York 1969.

[23] Trefethen L. N., Bau D., *Numerical linear algebra,* Siam, Philadelphia 1997.

[24] Tzou H. S., Tseng C. I., *Distributed modal identification and vibration control of continua: piezoelectric finite element formulation and analysis,* Journal of Dynamic Systems, Measurement and Control, Vol. 113, pp. 500- 505, 1991.

[25] Wang J., Yong Y.K., Imai T., *Finite element analysis of the piezoelectric vibrations of quartz plate resonators with higher-order plate theory,* Proceedings of 1997 IEEE International frequency control symposium, Orlando 1997.

[26] TICHÝ J., ZELENKA J., *Podélně a plošně střižně kmitajícípiezoelektrické rezonátory ze synthetického křemene*, s. as. Fys. 10, pp. 328 - 332, 1960.

[27] ZELENKA J., *Piezoelektrické rezonátory a jejich použití v praxi*, Academia, Praha 1981.

[28] LEHOUCQ R., MASCHHOFF K., SORENSEN D., YANG CH., `www.caam.rice.edu/software/ARPACK/`

[29] PAIGE C. C., SAUNDERS M. A., `http://www.stanford.edu/group/SOL/software/symmlq.html`

[30] MARQUES O., *SKYPACK User's Guide*, `http://crd.lbl.gov/~osni/#Software`

[31] MARQUES O., `http://crd.lbl.gov/~osni/#Software`

[32] `http://www.netlib.org/lapack`

[33] `http://www.geuz.org/gmsh/`

[34] `http://www.geuz.org/gmsh/doc/texinfo/gmsh.htm`

[35] `http://www.krystaly.cz`

[36] `http://www.sensortech.ca`

**Selected publications related to the topic of the thesis, written or participated by the author:**

[37] RÁLEK P., *Modelování piezoelektrických jevů*, Diploma thesis, FJFI, Czech Technical University, Prague 2001.

[38] MARYŠKA J., NOVÁK J., RÁLEK P., *Application of FEM in modelling of the resonance characteristics of piezoelectric resonators*, Proceedings of Algoritmy 2002, Slovakia, pp. 215-222, 2002.

[39] MARYŠKA J., NOVÁK J., RÁLEK P., *Finite element model of piezoelectric resonator*, Current Trends in Scientific Computing, Contemporary Mathematics, Vol. 329, pp. 263-270, 2003.

[40] MARYŠKA J., NOVÁK J., RÁLEK P., *Modelling of resonance characteristic of piezoelectric resonators - experimental experience*, Proc. 6th ECMS 2003, Liberec, pp.123-128, 2003.

[41] MARYŠKA J., NOVÁK J., RÁLEK P., *FEM model of piezoelectric continuum and selected applications*, Proceedings of the IMAMM 2003, Rožnov p. R., 2004.

[42] RÁLEK P., *Modelling of Piezoelectric Materials*, Proceedings of the IX. PhD. Conference ICS, AV R, 2004.

[43] RÁLEK P., *Generalized eigenvalue problem in modelling of the piezoelectric resonators*, Proceedings of Seminar on numerical analysis SNA '05, Ostrava, 2005.

[44] MARYŠKA J., NOVÁK J., RÁLEK P., *FEM modelling of the resonance frequencies of the planparallel quartz resonator*, Proceedings of ECMS 2005, Toulouse, 2005.

## Emendation:

page 80:

[42] RÁLEK P., *Modelling of piezoelectric materials*, Proceedings of the IX. PhD. Conference ICS, CAS, pp. 91–100, 2004.
[43] RÁLEK P., *Generalized eigenvalue problem in modelling of the piezoelectric resonators*, Proceedings of Seminar on numerical analysis SNA '05, Ostrava, pp. 68–71, 2005.

Papers [41] and [44] were issued on CD.